# Clathrin light chain directs endocytosis by influencing the binding of the yeast Hip1R homologue, Sla2, to F-actin

Douglas R. Boettner[a], Helena Friesen[b], Brenda Andrews[b], and Sandra K. Lemmon[a]
[a]Department of Molecular and Cellular Pharmacology, University of Miami, Miami, FL 33101; [b]Department of Molecular and Medical Genetics, University of Toronto, Toronto, ON M5S 1A8, Canada

**ABSTRACT** **The role of clathrin light chain (CLC) in clathrin-mediated endocytosis is not completely understood. Previous studies showed that the CLC N-terminus (CLC-NT) binds the Hip1/Hip1R/Sla2 family of membrane/actin–binding factors and that overexpression of the CLC-NT in yeast suppresses endocytic defects of clathrin heavy-chain mutants. To elucidate the mechanistic basis for this suppression, we performed synthetic genetic array analysis with a clathrin CLC-NT deletion mutation (*clc1-Δ19-76*). *clc1-Δ19-76* suppressed the internalization defects of null mutations in three late endocytic factors: amphiphysins (*rvs161* and *rvs167*) and verprolin (*vrp1*). In actin sedimentation assays, CLC binding to Sla2 inhibited Sla2 interaction with F-actin. Furthermore, *clc1-Δ19-76* suppression of the *rvs* and *vrp* phenotypes required the Sla2 actin-binding talin-Hip1/R/Sla2 actin-tethering C-terminal homology domain, suggesting that *clc1-Δ19-76* promotes internalization by prolonging actin engagement by Sla2. We propose that CLC directs endocytic progression by pruning the Sla2-actin attachments in the clathrin lattice, providing direction for membrane internalization.**

**Monitoring Editor**
Sandra L. Schmid
Scripps Research Institute

Received: Jul 19, 2011
Revised: Aug 4, 2011
Accepted: Aug 8, 2011

## INTRODUCTION

Clathrin is a major coat protein involved in vesicle formation during receptor-mediated endocytosis and sorting in the *trans*-Golgi network (TGN)/endosomal system (Traub, 2005). Clathrin is found as a triskelion containing three extended heavy chains (CHCs) trimerized at their C-termini and three light chains (CLCs). These assemble into a characteristic polyhedral coat on the cytosolic face of the membrane to facilitate clathrin-coated vesicle (CCV) formation. CHC interacts with adaptor proteins, which are involved in recruitment of clathrin to the membrane, as well as the binding to and sorting of cargo. Although the role of CHC in CCV formation is well established, the roles of CLC are not completely understood.

Previous work showed that CLCs bind along the vertex-proximal region of the CHC leg and are found on the outer surface of the clathrin lattice, where they are positioned to interact with other cytosolic and regulatory factors (Fotin *et al.*, 2004). They are important for stabilization of the mammalian triskelion hub fragments in vitro (Ybe *et al.*, 2003, 2007) and are essential for CHC trimerization in yeast (Chu *et al.*, 1996; Huang *et al.*, 1997). Biochemical studies also show that CLC inhibits spontaneous triskelion self-assembly (Ungewickell and Ungewickell, 1991; Liu *et al.*, 1995), and this activity depends on the conserved N-terminal acidic region of CLC (Ybe *et al.*, 1998). Recent work suggested that interaction of CLC or the CLC amino terminus with CHC might prevent the bending of the CHC knee that is required for lattice assembly (Wilbur *et al.*, 2010). However, depletion of CLC or overexpression of CLC lacking the N-terminal regulatory domain in animal cells has little effect on endocytosis, although some effect on TGN/endosomal sorting has been observed (Huang *et al.*, 2004; Chen and Brodsky, 2005; Poupon *et al.*, 2008; Wilbur *et al.*, 2008).

The CLC N-terminal acidic region also interacts with the central coil-coiled dimerization domain of the Hip1/Hip1R/Sla2 family of proteins (Chen and Brodsky, 2005; Legendre-Guillemin *et al.*, 2005; Newpher *et al.*, 2006). Some evidence suggests that Hip1/R binding to CLC promotes clathrin assembly by releasing the CLC

This article was published online ahead of print in MBoC in Press (http://www.molbiolcell.org/cgi/doi/10.1091/mbc.E11-07-0628) on August 17, 2011.

Address correspondence to: Sandra K. Lemmon (Slemmon@med.miami.edu).

Abbreviations used: CHC, clathrin heavy chain; CLC, clathrin light chain; GFP, green fluorescent protein; NT, N-terminus; RFP, red fluorescent protein; SGA, synthetic genetic array; THATCH, talin-Hip1/R/Sla2 actin-tethering C-terminal homology; *ts*, temperature sensitive.

© 2011 Boettner *et al*. This article is distributed by The American Society for Cell Biology under license from the author(s). Two months after publication it is available to the public under an Attribution–Noncommercial–Share Alike 3.0 Unported Creative Commons License (http://creativecommons.org/licenses/by-nc-sa/3.0).
"ASCB®," "The American Society for Cell Biology®," and "Molecular Biology of the Cell®" are registered trademarks of The American Society of Cell Biology.

N-terminal negative regulation on CHC (Chen and Brodsky, 2005; Legendre-Guillemin *et al.*, 2005). Because Hip1-related proteins contain both an AP180 N-terminal homology domain (ANTH) that binds membrane-associated phosphatidyl inositides and a talin/Hip1/R/Sla2 actin-tethering C-terminal homology domain (THATCH) that binds F-actin, they may provide a critical link between the membrane and the actin cytoskeleton or regulate actin assembly during clathrin-mediated transport (McCann and Craig, 1997; Yang *et al.*, 1999; Legendre-Guillemin *et al.*, 2002; Hyun *et al.*, 2004; Senetar *et al.*, 2004; Sun *et al.*, 2005; Brett *et al.*, 2006; Wilbur *et al.*, 2008). Depletion of Hip1 family proteins from cells leads to aberrant actin assemblies at clathrin-coated membranes in both yeast and animal cells (Kaksonen *et al.*, 2003; Engqvist-Goldstein *et al.*, 2004; Newpher *et al.*, 2005; Le Clainche *et al.*, 2007; Poupon *et al.*, 2008), and similarly treatments that affect the ability of CLC to interact with Hip1R in animal cells perturb actin structures at clathrin-coated membranes (Chen and Brodsky, 2005; Poupon *et al.*, 2008; Wilbur *et al.*, 2008; Saffarian *et al.*, 2009). Still, the role of CLC regulation of Hip1 family proteins remains unclear.

Yeast provides elegant ways to address these questions by combining live-cell imaging with powerful molecular genetic tools. This model system has established a spatiotemporal map from recruitment to disassembly and is now elucidating details about the molecular functions of a large number of endocytic factors. Clathrin-mediated endocytosis in yeast takes place at cortical patches and involves many factors that have animal cell counterparts (Engqvist-Goldstein and Drubin, 2003; Robertson *et al.*, 2009; Galletta *et al.*, 2010). Generally the process has an immobile stage for establishing the endocytic site and a rapid, mobile phase when invagination and vesicle formation occur. During the immobile phase (1–2 min) several endocytic coat factors and adaptors collect at a cortical patch, including the F-BAR domain protein Syp1 (FCHO1/FCHO2 homologue), Ede1 (an Eps15 homology [EH] domain protein), and clathrin (Newpher *et al.*, 2005; Boettner *et al.*, 2009; Reider *et al.*, 2009; Stimpson *et al.*, 2009). Later in the immobile phase Sla2 (Hip1/Hip1R) appears, followed by Sla1 (an SH3 domain–containing protein), the two EH domain factors Pan1 and End3, and the WASp homologue, Las17 (Kaksonen *et al.*, 2003, 2005; Newpher and Lemmon, 2006). Many actin-binding or -remodeling proteins, such as Abp1, capping protein, and Arp2/3 complex, appear or are activated during the mobile phase, which lasts only 10–15 s (Kaksonen *et al.*, 2003, 2005). At the onset of the mobile phase, the WIP homologue, verprolin (Vrp1), localizes to the cortical site, where it recruits and activates the type-I myosins (Myo3/5), which are potent Arp2/3 activators believed to produce a final burst of actin needed to drive invagination (Kaksonen *et al.*, 2003, 2005; Jonsdottir and Li, 2004; Sun *et al.*, 2006; Galletta *et al.*, 2008). When the patch has invaginated 200–300 nm, the vesicle pinches off, facilitated by the N-BAR domain amphiphysin homologues Rvs161 and Rvs167, uncoating occurs, and the vesicle associated with actin moves deeper into the cell (Kaksonen *et al.*, 2003, 2005).

Here we explore how the CLC N-terminus (CLC-NT) regulates the yeast Hip1R homologue, Sla2. Sla2 arrives at endocytic sites well after clathrin, so it is not required for assembly of clathrin (Newpher *et al.*, 2006; Newpher and Lemmon, 2006). As in mammalian cells, deletion of *SLA2* leads to accumulation of early coat factors at the cortex and unproductive actin comet tails emanating from these sites (Kaksonen *et al.*, 2003; Newpher *et al.*, 2005). Our previous work discovered that *CLC1*, which encodes CLC, is a high-copy suppressor of clathrin HC–deficient (*chc1*Δ) yeast, indicating that CLC possesses regulatory functions during endocytosis (Huang *et al.*, 1997). Furthermore, we isolated Sla2 as a CLC-interacting protein (Henry *et al.*, 2002); as in animal cells, the yeast CLC-NT interacts with the coiled-coiled domain of Sla2 (Newpher *et al.*, 2006; Newpher and Lemmon, 2006). Of interest, overexpression of the N-terminal Sla2-binding region of CLC suppresses the endocytic phenotypes of clathrin-null mutants, including progression of stalled Sla2-containing endocytic patches (Newpher *et al.*, 2006). However, deletion of the CLC-NT alone has minimal effect on its own, likely due to redundancy of the endocytic machinery.

To further investigate the regulatory role of CLC during endocytic progression we took advantage of the genome-wide synthetic genetic array (SGA) approach (Tong and Boone, 2006), using a *clc1* mutant encoding CLC lacking the Sla2-binding region (*clc1-*Δ*19-76*) as the query strain. To our surprise, the *clc1-*Δ*19-76* allele alleviated growth defects of null mutants for three late endocytic factors: verprolin (Vrp1) and the amphiphysins (Rvs161 and Rvs167). Our analysis of this suppression by live-cell imaging, combined with biochemical evidence, suggests that CLC negatively regulates Sla2 binding to the actin cytoskeleton to restrict the number and/or location of Sla2's actin attachments to promote internalization.

## RESULTS

### Synthetic genetic array analysis with *clc1-*Δ*19-76*

We present the first SGA screen performed on a clathrin mutant. Genetic analysis of clathrin mutants previously were limited to small-scale screens (Bensen *et al.*, 2000, 2001), and large-scale SGA analysis was not done because clathrin-null yeast (*clc1*Δ or *chc1*Δ) exhibit massive polyploidy (Lemmon *et al.*, 1990; Huang *et al.*, 1997), which renders them unreliable participants in these screens. To explore the mechanism of CLC regulation of endocytosis, we generated a strain (SL5677) for SGA analysis carrying an integrated mutation, *clc1-*Δ*19-76*, encoding CLC lacking the Sla2-binding residues (Figure 1A). CLC expression from *clc1-*Δ*19-76* was essentially the same as from wild-type *CLC1*; however, clathrin HC levels appeared to be slightly decreased in these cells (Figure 1, B and C). Except for a slight cold sensitivity (unpublished data), *clc1-*Δ*19-76* yeast were similar to wild-type yeast in all tests performed (see later discussion).

For SGA analysis *clc1-*Δ*19-76* was first systematically crossed to a collection of 177 temperature-sensitive (*ts*) alleles enriched for genes encoding proteins involved in membrane trafficking, endocytosis, and actin function (listed in Supplemental Table S1B). This screen identified 11 genes whose mutations caused synthetic growth defects in the presence of the *clc1* mutation, including the endocytic coat factor Pan1 and the Arp2/3 complex subunit Arp3 (Figure 1G), although the latter showed major differences, depending on the *arp3* allele, and might be complicated by additional functions of the Arp2/3 complex, for example, mitochondrial movement (Boldogh *et al.*, 2001). We confirmed the *pan1* genetic interaction with an additional allele, *pan1-20*, which was in fact synthetic lethal with *clc1-*Δ*19-76* (Supplemental Figure S1A). A larger-scale SGA screen involved crossing the *clc1-*Δ*19-76* mutant to 3885 strains from the viable deletion collection. This screen identified 336 aggravating mutations (synthetic growth phenotypes; Supplemental Table S3B) and 58 mutants whose growth phenotypes were alleviated by *clc1-*Δ*19-76* (synthetic rescue phenotypes; Table 1A and Supplemental Table S3A).

Gene ontology categories were used to sort the data set by biochemical processes (Supplemental Table S2). Fifteen percent of genes identified by the deletion screen were associated with the Gene Ontology term "vesicle transport," in vast excess of the expected 5% found in the genome ($p \leq 7 \times 10^{-11}$). Several protein complexes showed statistically significant representation in our data

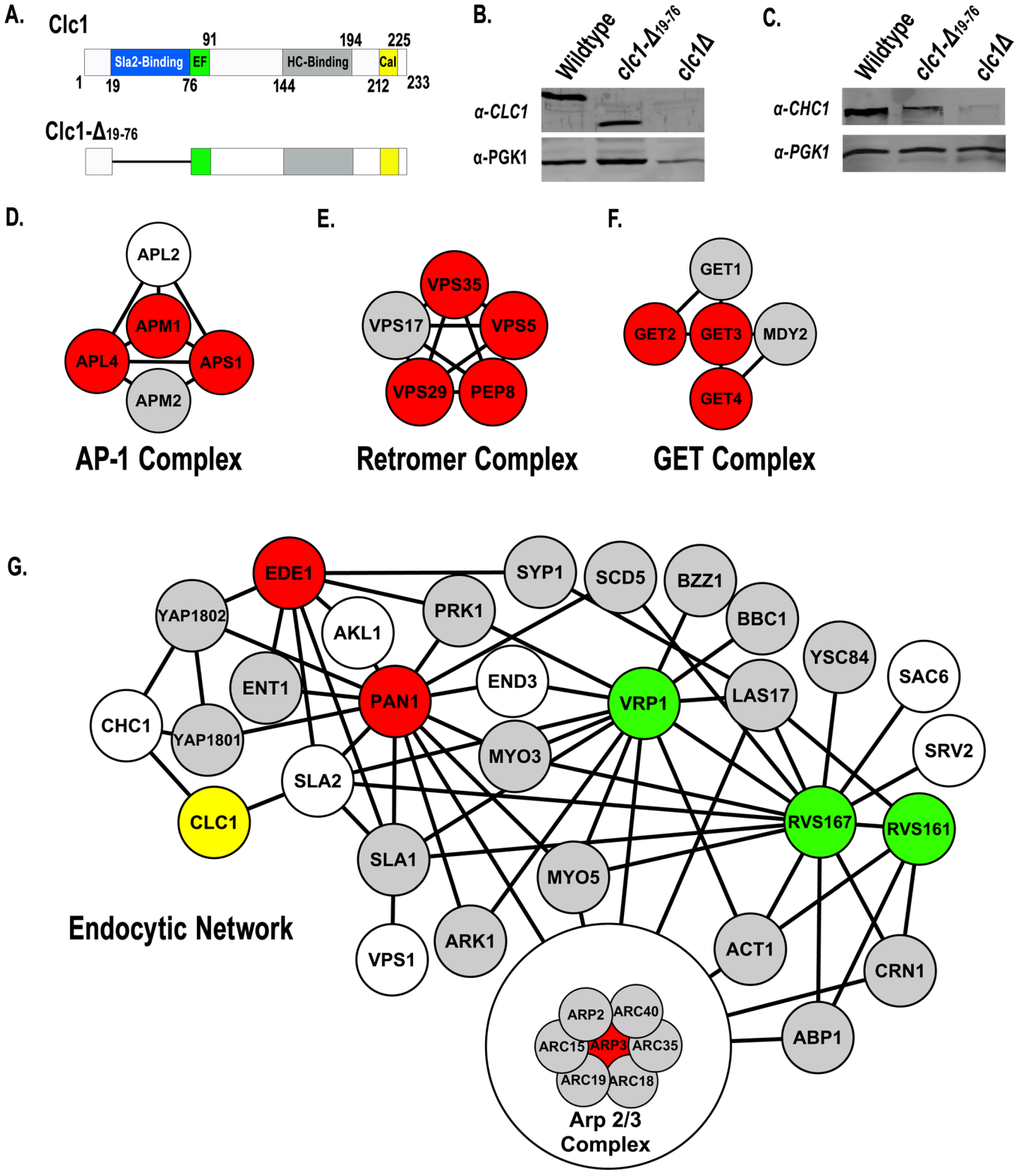


FIGURE 1: Synthetic genetic array analysis with the *clc1-Δ19-76* allele. (A) Schematics of Clc1 and Clc1-Δ19-76, highlighting regions that bind Sla2 (blue), CHC (gray), or calmodulin (yellow) and the region comprising an EF hand motif (green). (B) Immunoblot of protein extracts from wild type (SL1462), *clc1-Δ19-76* (SL5677), and *clc1Δ* (SL1620) probed with anti-Clc1 and anti-Pgk1 (loading control). (C) Same as B, but probed with anti-Chc1 monoclonal antibodies. (D–G) Edges represent published physical protein–protein interactions; nodes are white if they were not in the screen and gray if no interaction was identified. If double mutants produced a synthetic growth defect relationship, they are labeled in red, and nodes demonstrating synthetic rescue with *clc1-Δ19-76* are labeled in green. (D) *clc1-Δ19-76* demonstrated a relationship with three AP-1–complex subunits ($p \leq 0.01$). (E) Four of the five core retromer complex proteins were identified ($p \leq 0.01$). (F) Three of the five components of the GET complex were identified ($p \leq 0.01$). (G) Endocytic network showing hits from SGA analysis with *clc1-Δ19-76*.

| Gene | Description (homologue) |
|---|---|
| **A. Null mutations showing synthetic rescue with *clc1-Δ19-76*[a]** | |
| VRP1 | WASp-interacting protein 1, regulates myosin I (WIP) |
| VPH1 | V-type proton ATPase 116-kDa subunit A |
| YMR166C | Mitochondrial ATP-Mg/$P_i$ carrier |
| ELM1 | Ser/Thr protein kinase, regulates morphogenesis and cytokinesis |
| ROD1 | Art4, α-arrestin |
| CBF1 | Centromere-binding factor |
| FIS1 | Mitochondrial fission protein (Fis1) |
| EST1 | Telomere elongation (hEST1A, hEST1B) |
| RPL14A | Ribosomal protein L14 (RPL14) |
| RVS167 | BIN1/amphyphisin/endophilin |
| SIN3 | Histone deacetylase complex (SIN3A) |
| LSM6 | Like SM-protein involved in mRNA decay, U6 snRNP component |
| CEX1 | tRNA export from nucleus |
| SHE4 | Binds unconventional myosins |
| VAC14 | Regulation of phosphatidylinositol 3,5-bisphosphate synthesis (hVAC14) |
| ARL1 | ADP-ribosylation factor–like; TGN–endosomal transport (ARL) |
| CSE2 | RNA polymerase II transcription mediator complex |
| GAP1 | General amino acid permease |
| EMI5 | Succinate dehydrogenase subunit |
| BRR1 | Component of spliceosomal snRNPs |
| ECM8 | Unknown |
| FMP23 | Unknown |
| PMA2 | Plasma membrane $H^+$ ATPase |
| MAP2 | Methionine aminopeptidase (METAP2) |
| HOM6 | Homoserine dehydrogenase |
| CPR7 | Peptidyl-prolyl *cis–trans* isomerase |
| PEX27 | Peripheral peroxisomal membrane protein |
| UBP6 | Ubiquitin-specific protease of proteosome (USP14) |
| BER1 | Unknown |
| SNU66 | Component of the U4/U6.U5 snRNP complex |
| PAT1 | Deadenylation-dependent mRNA-decapping factor |
| RVS161 | BIN1/amphyphisin/endophilin |
| SYS1 | Golgi membrane protein |
| **B. *ts* mutants showing synthetic growth defects with *clc1-Δ19-76*[b]** | |
| ALG2 | Mannosyltransferase (ALG2) |
| ARP3 | Component of the Arp2/3 complex (ACTR3B) |
| COP1 | α subunit of COPI coatomer complex (COPA) |
| LST8 | Torc1/2 component |
| MCD4 | Involved in GPI anchor synthesis (PIGN) |
| PAN1 | EH domain containing endocytic factor |
| PIK1 | Phosphatidylinositol 4-kinase |
| SEC2 | Post-Golgi GEF for Sec4 |
| SEC21 | γ subunit of coatomer (COPG2) |
| YIF1 | Fusion of ER-derived COPII vesicles (YIF1A) |
| YIP1 | Fusion of ER-derived COPII vesicles (YIPF5) |

snRNP, small nuclear ribonucleoprotein.
[a]Genes whose null mutation caused synthetic rescue phenotypes in combination with *clc1-Δ19-76* with an $\varepsilon > 0.180$ and $p < 0.015$. Results are ranked by ε score. Verprolin (*VRP1*) and both amphiphysins (*RVS167* and *RVS161*) are highlighted in red.
[b]Genes with an adjusted calibrated p between 0.1 and 1, ranked by this value.

TABLE 1: Selected genes identified by SGA screens.

(i.e., greater than expected for the size of the data set). Included was the clathrin-associated TGN/endosomal AP-1 adaptor complex ($p < 0.01$; Figure 1D). These negative genetic interactions are consistent with previous work combining clathrin and AP-1 adaptor mutations (Stepp *et al.*, 1995; Yeung *et al.*, 1999). Negative genetic interactions were also observed with a number of other factors involved in retrograde transport from the endosome to the TGN (Supplemental Table S2), including most components of the retromer complex (Figure 1E; $p < 0.01$). We hypothesize that this exacerbated growth phenotype was caused by impairment of two parallel retrograde pathways from the endosome, one involving clathrin and another involving retromer. In addition, we identified several subunits of the GET complex, which is required for insertion of tail-anchored proteins into the endoplasmic reticulum (ER) (Simpson *et al.*, 2010) (Figure 1F; $p < 0.01$). GET complex–requiring soluble *N*-ethylmaleimide–sensitive factor attachment protein receptors, such as SNC2 and VAM3, were also identified, suggesting that GET complex interactions may just phenocopy the loss of these downstream targets.

In accordance with the previously described clathrin synthetic lethality screen using a *ts chc1* allele, *chc1-521* (Bensen *et al.*, 2000, 2001), we identified four mutants (*ric1*, *gga1*, *vps21*, and *inp53*) with synthetic growth defects in combination with *clc1-Δ19-76*. We suspect that some of these negative genetic interactions with the *clc1* mutant may be related to the reduced levels of Chc1; however, we cannot rule out that the CLC-NT has some TGN/endosomal–specific function. Genetic interactions involving mutations affecting other stages of the secretory/endosomal transport pathways and a number of membrane transporters were identified (Supplemental Table S2). Others were observed with genes important for cell wall biosynthesis, glycosylation, lipid/sphingolipid and phosphatidyl inositide synthesis, and components affecting ubiquitin modification. The last-named observation is consistent with previous studies showing that clathrin-deficient yeast accumulate ubiquitinated conjugates and deplete cellular ubiquitin stores (Nelson and Lemmon, 1993).

In addition to *pan1* and *arp3* found in the *ts* screen, a null allele of *EDE1*, which encodes an EH-domain early endocytic adaptor, caused synthetic growth defects in combination with *clc1-Δ19-76* (Figure 1G). Most interesting was that *clc1-Δ19-76* suppressed the growth defects of null mutations for three late-stage endocytic factors: Vrp1 (verprolin, the type I myosin activator related to WIP) and Rvs161 and Rvs167 (amphiphysins involved in vesicle scission; Figure 1G and Table 1). These unusual positive genetic interactions seemed more likely to yield mechanistic insight into the role of the CLC-NT. Thus we focused primarily on *vrp1* and *rvs167* since their ε scores were high, but *rvs161* gave similar, although more subtle effects, as shown for *rvs167*.

### The *clc1-Δ19-76* allele suppresses growth and endocytic defects of *vrp1Δ* and *rvs167Δ*

To ensure the validity of these genetic interactions, the *clc1-Δ19-76* mutation was recapitulated in our SL1462 lab strain and crossed to either *vrp1Δ* or *rvs167Δ*. Whereas *clc1-Δ19-76* yeast grew well at 30 or 37°C, *vrp1* (Figure 2A) and *rvs167Δ* (Figure 2B) cells were *ts* at 37°C. Consistent with the SGA screen, *clc1-Δ19-76* suppressed the *ts* growth of *vrp1Δ* (Figure 2A) and *rvs167Δ* (Figure 2B) at 37°C. Actin polarity defects are often associated with endocytic mutations. *clc1-Δ19-76* cells were polarized like wild type, and the *clc1* allele substantially suppressed the polarity defects caused by *vrp1Δ* or *rvs167Δ* as well (Figure 2, C and D).

Lucifer yellow (LY) uptake assays were used to test bulk fluid-phase endocytosis (Figure 2, E and F). LY uptake in the *clc1-Δ19-76* mutant was similar to wild type. As expected, both *vrp1Δ* and *rvs167Δ* yeast had minimal uptake, with only 5–8% of cells with labeled vacuoles. However, when combined with the *clc1-Δ19-76* allele there was significant restoration of LY internalization compared with either null allele alone (Figure 2, E and F). Similarly the LY uptake defect in *rvs161Δ* was suppressed by *clc1-Δ19-76* (Supplemental Figure S1B). Because we saw no defect in growth at elevated temperature, polarity, or LY uptake in the *clc1-Δ19-76* mutant alone, we conclude that this mutation suppresses the defects caused by the verprolin or amphiphysin gene deletions.

### *clc1-Δ19-76* rescues *vrp1Δ* defects in endocytic dynamics and inward vesicle movement

Previous reports showed that verprolin arrives at the endocytic patch just prior to the actin phase, where it plays a role in the recruitment and activation of the potent Arp2/3–activating type I myosins (Myo3 and Myo5), which are important for actin-dependent membrane invagination (Anderson *et al.*, 1998; Evangelista *et al.*, 2000; Geli *et al.*, 2000; Sirotkin *et al.*, 2005; Sun *et al.*, 2006). Thus, inward movement of endocytic patches is defective in *vrp1Δ* yeast because of reduced Myo3/5 at the patch and impaired activation of residual myosin present (Sun *et al.*, 2006). To visualize whether *clc1-Δ19-76* suppressed the defects of *vrp1Δ*, we combined these mutations with early endocytic markers (either Sla2–green fluorescent protein [GFP] or Sla1-GFP) and a mobile phase/actin marker (Abp1–red fluorescent protein [RFP]), and collected time-lapse movies of their dynamics in live cells. Unlike growth defects, which were best observed at elevated temperatures, the endocytic defects of *vrp1Δ* (and *rvsΔ*; see later discussion) were highly penetrant, so movies were taken at 25°C.

The *clc1-Δ19-76* mutation alone caused no significant change in the lifetime of any endocytic marker we tested, and invagination was normal (Figure 3, A–C, and unpublished data). In contrast, *vrp1Δ* yeast demonstrated dramatic lifetime elongation of both Sla1-GFP and Sla2-GFP (Figure 3, A–C). Sla1-GFP lifetimes were prolonged from 31 ± 6 s in wild type to 69 ± 17 s in *vrp1Δ* ($p < 0.0001$; Figure 3, A and C). Sla2-GFP was more severely affected, with lifetimes extended from 49 ± 15 s in wild type to 165 ± 57 s in the verprolin mutant ($p \leq 0.0001$; Figure 3, B and C). Combining *clc1-Δ19-76* with *vrp1Δ* significantly reduced the lifetimes of both Sla1-GFP (to 56 ± 14 s; $p \leq 0.001$) and Sla2-GFP (to 73 ± 25 s; $p \leq 0.0001$; Figure 3, A–C). Of note, there was also an elongation of the actin stage of endocytosis in *vrp1Δ*, as marked by Abp1-RFP, but this was not suppressed by the *clc1-Δ19-76* mutation.

The invagination defect caused by *vrp1* was also suppressed by *clc1-Δ19-76*. In *vrp1Δ* 80% of Sla2 patches accumulated some degree of Abp1-RFP (Figure 3, D–F), but only 20% of these showed any movement inward from the cortex. This percentage increased to 47% in *vrp1Δ clc1-Δ19-76* (Figure 3, D–E). This was also seen in single-particle tracking of movement of Sla2-GFP, which normally invaginates 200–300 nm with the forming vesicle and disassembles shortly after vesicle scission. The depth of Sla2-GFP inward movement was impeded in *vrp1Δ* (65 ± 13 nm vs. 250 ± 20 nm in wild type, $n = 10$), but this was restored to near wild-type distances (190 ± 43 nm, $n = 10$) in *vrp1Δ clc1-Δ19-76* (Figure 3F).

### *clc1-Δ19-76* rescues *rvs167Δ* defects in endocytic dynamics

Rvs161 and Rvs167 form a heterodimer through their N-terminal N-BAR domain and are recruited late to endocytic sites (Kaksonen *et al.*, 2005; Friesen *et al.*, 2006). These proteins require one another for stable expression, and deletion of either of these proteins causes endocytic defects (Munn *et al.*, 1995; Lombardi and Riezman, 2001; Friesen *et al.*, 2006). Notable in amphiphysin-null mutants is a

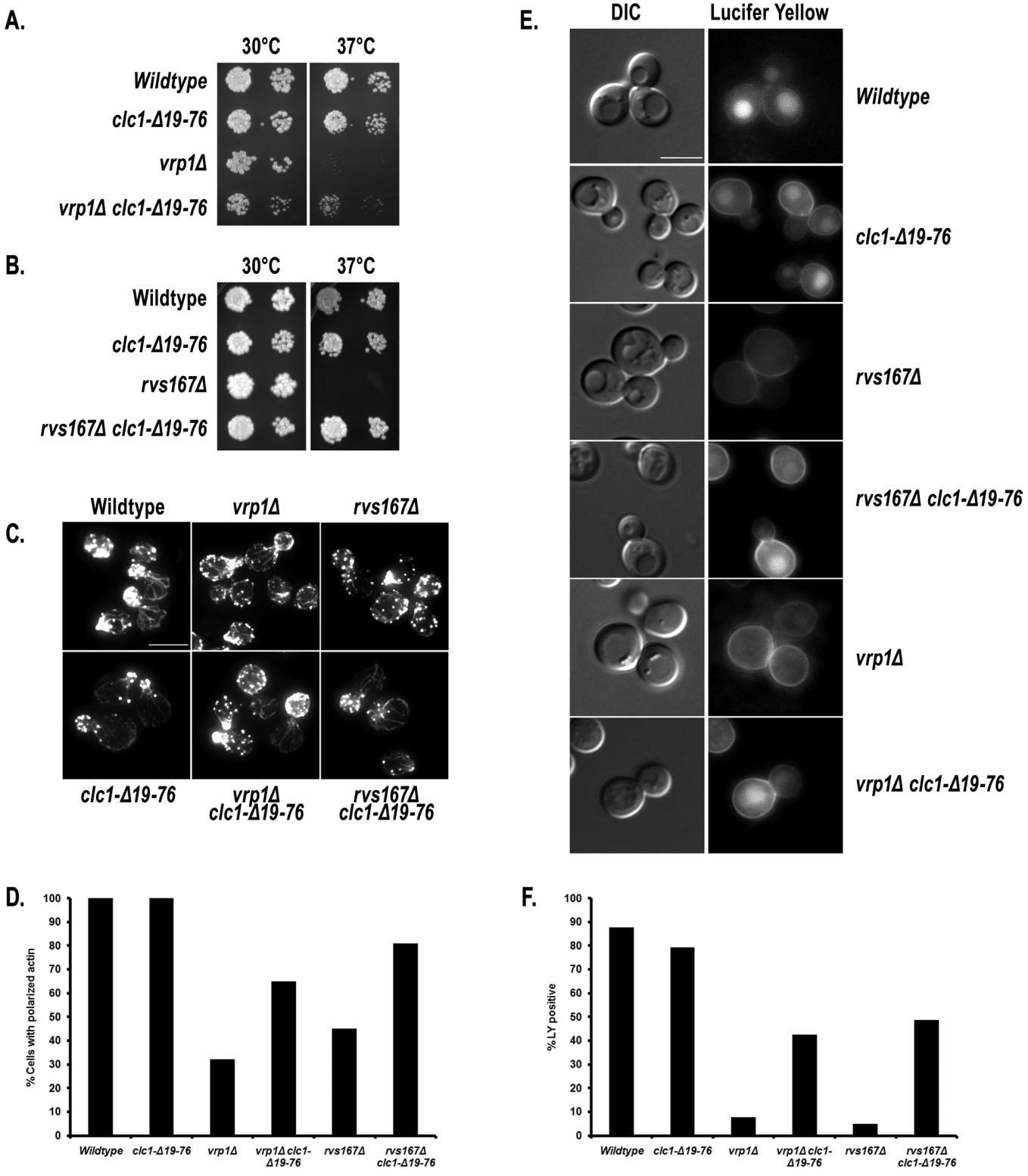


FIGURE 2: *clc1-Δ19-76* suppresses the growth, actin polarity, and fluid-phase endocytosis defects of verprolin and amphiphysin null mutants. (A) Growth with *vrp1Δ*: wild type (SL1462), *clc1-Δ19-76* (SL6044), *vrp1Δ* (SL4136), and *vrp1Δ clc1-Δ19-76* (SL6049) were fivefold serially diluted, plated on YEPD, and grown at 30 or 37°C for 60 h. (B) Growth with *rvs167Δ*: wild type (SL1462), *clc1-Δ19-76* (SL6044), *rvs167Δ* (RH2951), and *rvs167Δ clc1-Δ19-76* (SL6052) were plated and grown as in A. (C) Actin polarization: strains shown in A and B were grown at 25°C, fixed, and stained with Alexa Fluor 568–phalloidin. Each image is a max-Z projection of 12 (0.2 μm) optical sections after nearest-neighbor deconvolution (bar, 5 μm). (D) Quantification of actin polarization reported as percentage of small and medium budded cells with >50% of phalloidin stain in the bud (n = 75). (E) Example micrographs of strains indicated in A and B after Lucifer yellow (LY) uptake for 1 h at 25°C (bar, 5 μm). (F) Quantification of LY uptake reported as percentage of cells with vacuolar LY (n = 90).

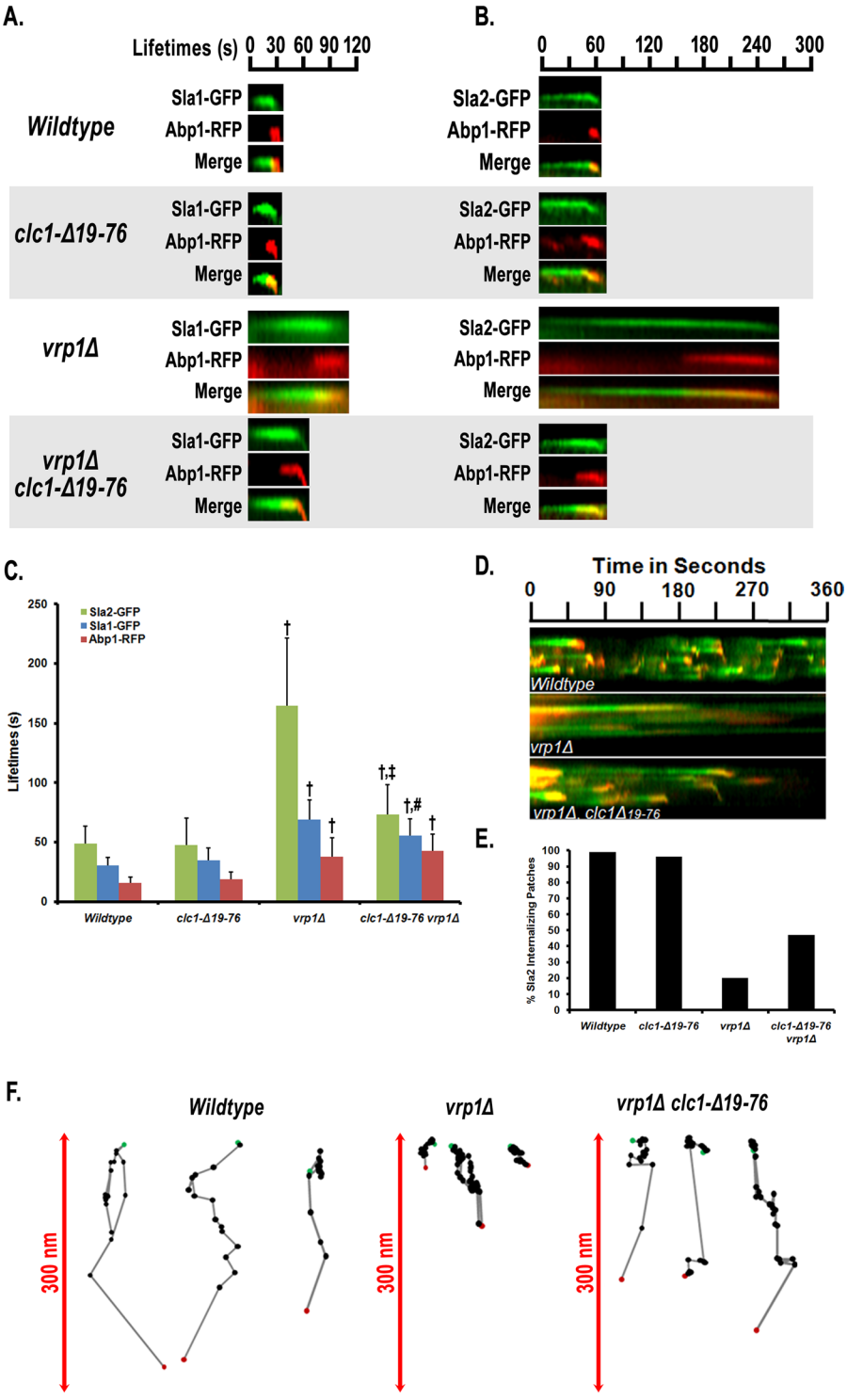


FIGURE 3: Defects in endocytic dynamics of *vrp1*Δ are suppressed when combined with *clc1-*Δ*19-76*. (A) Representative kymographs of Sla1-GFP/Abp1-RFP patches in wild type (SL5311), *clc1-*Δ*19-76* (SL6068), *vrp1*Δ (SL6065), and *vrp1*Δ *clc1-*Δ*19-76* (SL6062). (B) Representative kymographs of Sla2-GFP/Abp1-RFP patches in wild type (SL5927), *clc1-*Δ*19-76* (SL6084), *vrp1*Δ (SL6081), *vrp1*Δ *clc1-*Δ*19-76* (SL6077). (C) Fluorescence lifetimes of Sla2-GFP, Sla1-GFP, and Abp1-RFP in strains shown in A and B. Data are reported as average ± SD (n ≥ 50). †p ≤ 0.0001 vs. wild type; ‡p ≤ 0.0001 vs. *vrp1*Δ; #p ≤ 0.001 vs. *vrp1*Δ. (D) Tangential kymographs illustrating inward movement of Sla2-GFP/Abp1-RFP endocytic patches in wild type, *vrp1*Δ, and *vrp1*Δ *clc1-*Δ*19-76*. (E) Percentage of Sla2-GFP/Abp1-RFP patches that demonstrate "normal" inward movement (n = *90*). (F) Example plots of Sla2-GFP trajectories comparing inward movement from wild type, *vrp1*Δ, and *vrp1*Δ *clc1-*Δ*19-76*. Each point represents a 2-s frame, with the length of the lines between frames indicating distance moved. Initial coordinates are highlighted in green, and the final time points are in red.

retraction behavior, in which endocytic patches begin to internalize but then return to the cell cortex and dissipate, consistent with a role in vesicle scission (Kaksonen *et al.*, 2005; Youn *et al.*, 2010).

By time-lapse imaging we found that Sla2-GFP lifetimes were lengthened by twofold in *rvs167*Δ, but the *clc1-*Δ*19-76* allele restored Sla2 lifetimes to near wild type (99 ± 33 vs. 54 ± 21 s, p ≤ 0.0001, *rvs167*Δ vs. *rvs167*Δ *clc1-*Δ*19-76*, respectively) (Figure 4, B and C). The *clc1-*Δ*19-76* mutation also significantly reduced the lifetimes of Sla1-GFP (51 ± 14 vs. 44 ± 13 s, p ≤ 0.03, *rvs167*Δ vs. *rvs167*Δ *clc1-*Δ*19-76*, respectively; Figure 4, A and C). Similar although more subtle results were obtained in *rvs161*Δ yeast (Supplemental Figure S1C). In addition, combining the *clc1-*Δ*19-76* allele with either *rvs167*Δ or *rvs161*Δ increased the number of internalizing patches and reduced the retraction of endocytic markers back to the cortex as compared with either *rvs* mutant alone (Figure 4D and Supplemental Figure S1D).

## Neither *vrp1*Δ nor *rvs167*Δ is suppressed by *clc1*Δ

To test whether the suppression by *clc1-*Δ*19-76* was unique to this *clc1* allele and not due to general loss of CLC function or the slightly reduced levels of clathrin HC, we tested the ability of the null *clc1*Δ to suppress *vrp1*Δ or *rvs167*Δ growth and endocytosis. In either case neither temperature sensitivity nor endocytic dynamics was rescued (Figure 5). The endocytic profiles seen in *vrp1*Δ *clc1*Δ yeast were more characteristic of a clathrin-null than a verprolin-null mutant (Newpher and Lemmon, 2006) since nearly 77% of Sla2-GFP patches persisted longer than 360 s (Figure 5B). Of interest, the characteristic actin comet tails caused by *clc1*Δ were missing in *vrp1*Δ *clc1*Δ cells, probably due to impaired recruitment of the type I myosins in *vrp1* and, as a consequence, reduced actin assembly. *rvs167*Δ *clc1*Δ cells also had severe endocytic defects (Figure 5D). Again, 77% of all Sla2-GFP patches were arrested, and in these cells dramatic actin comet tails were evident in 23% of patches.

## *clc1-*Δ*19-76* suppression of *vrp1*Δ and *rvs167*Δ requires actin binding by Sla2

As shown earlier, deletion of the N-terminus of CLC suppressed the loss of Vrp1 and Rvs proteins, three components of the actin phase of internalization. Because CLC-N terminus binds directly to the Sla2 coiled-coil region and Sla2 binds directly to F-actin through its THATCH domain, we considered the possibility that the *clc1-*Δ*19-76* mutant effects were mediated through altered ability to regulate Sla2 actin binding. Therefore we examined the effect of CLC on Sla2 in vitro using F-actin

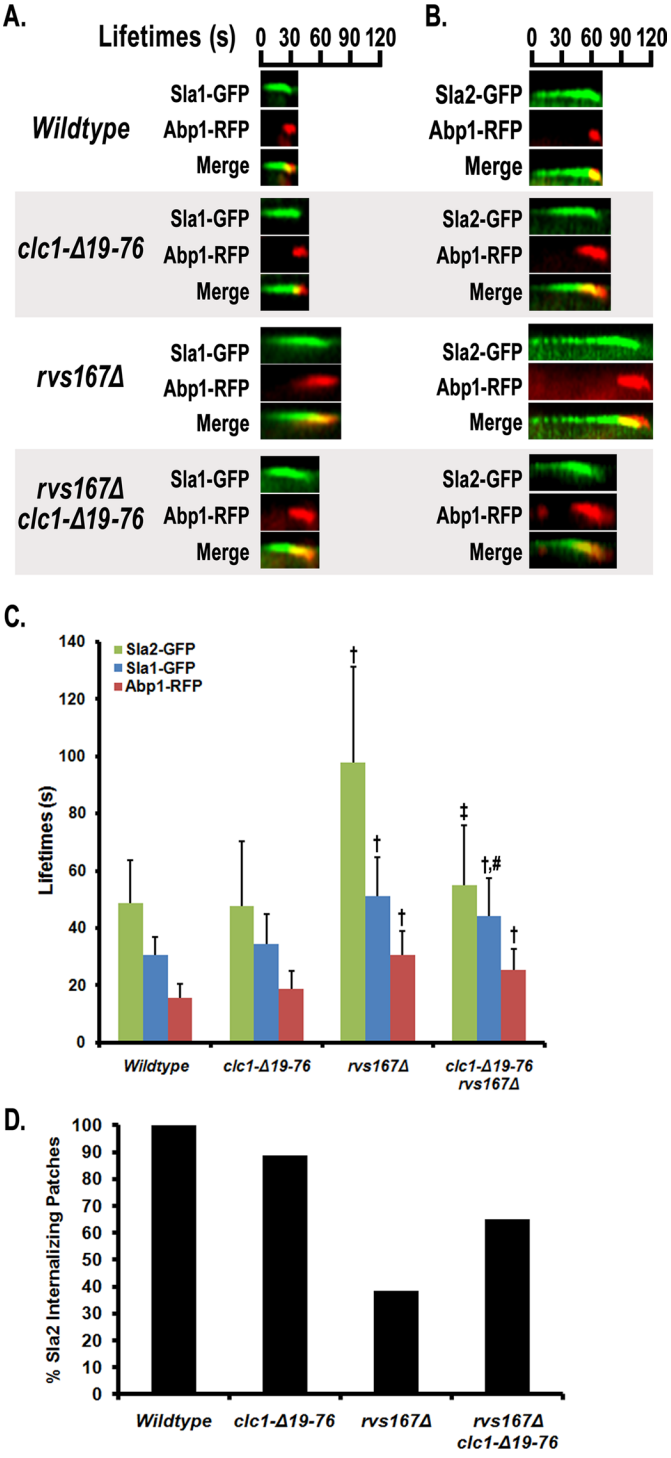


FIGURE 4: Defects in endocytic dynamics of *rvs167*Δ are suppressed when combined with *clc1-Δ19-76*. (A) Representative kymographs of Sla1-GFP/Abp1-RFP patches in wild type (SL5311), *clc1-Δ19-76* (SL6068), *rvs167*Δ (SL6108), and *rvs167*Δ *clc1-Δ19-76* (SL6191). (B) Representative kymographs of Sla2-GFP/Abp1-RFP patches in wild type (SL5927), *clc1-Δ19-76* (SL6084), *rvs167*Δ (SL6196), and *rvs167*Δ *clc1-Δ19-76* (SL6197). (C) Fluorescence lifetimes of Sla2-GFP, Sla1-GFP, and Abp1-RFP in strains shown in A and B. Data are reported as average ± SD (n ≥ 50). †p ≤ 0.0001 vs. wild type; ‡p ≤ 0.0001 vs. *rvs167*Δ; #p ≤ 0.03 vs. *rvs167*Δ. (D) Percentage of patches that show "normal" inward movement following Abp1 accumulation (n = 90). Similar results were obtained for *rvs161*Δ (see Supplemental Figure S1).

cosedimentation assays. Purified glutathione *S*-transferase (GST) fusions of Sla2 (Figure 6A) were incubated with preassembled F-actin and pelleted at high speed (Figure 6, B and C, and Supplemental Figure S2). All Sla2 fragments with the THATCH domain bound to F-actin. When the clathrin LC–binding site was present (GST-Sla2-292-968), preincubation with a 5 M excess of histidine (His)6-tagged-LC (6xHis-Clc1) reduced cosedimentation dramatically (Figure 6B and Supplemental Figure S2D). Similar results were found for full-length GST-Sla2 (Supplemental Figure S2, A and D); however, in our hands GST-Sla2 was considerably less stable and less soluble than fragments lacking the ANTH domain (unpublished data). In contrast, the THATCH domain alone (GST-Sla2-717-968), lacking the clathrin LC–binding region, bound actin even in the presence of 6xHis-Clc1 (Figure 6C and Supplemental Figure S2D). GST-Crn1 (coronin) was tested as a positive control for F-actin binding and was found to bind actin in the presence or absence of Clc1 (Supplemental Figure S2D and unpublished data). Neither bovine serum albumin contained in the actin-binding buffer (Supplemental Figure S2C) nor GST (unpublished data) bound nonspecifically to F-actin. Overall these results indicate that CLC inhibits the ability of Sla2 to bind to actin.

To determine whether *clc1-Δ19-76* suppression of *vrp1*Δ or *rvs167*Δ in vivo was mediated through Sla2, we tested whether the Sla2 C-terminal THATCH domain was required for this effect. A hemagglutinin (HA) tag was inserted at residue 717 of Sla2, causing a C-terminal truncation. As a control, an HA tag was inserted after the full-length Sla2 coding sequence. Deletion of the THATCH region caused no phenotype (unpublished data), as shown previously (Wesp *et al.*, 1997; Yang *et al.*, 1999). However, although *vrp1*Δ *clc1-Δ19-76* or *rvs167*Δ *clc1-Δ19-76* cells could grow at 37°C, triple-mutant cells also containing the *sla2-Δthatch* allele were *ts* for growth (Figure 6D). Collectively these data indicate that the suppression by *clc1Δ19-76* depends on the interaction of Sla2 with F-actin through the Sla2 THATCH domain.

### *clc1-Δ19-76* suppresses mutations in major actin nucleation–promoting factors

At the endocytic patch F-actin is densely branched, requiring the Arp2/3 complex for assembly (Goode and Rodal, 2001). The Arp2/3 complex has little activity on its own since it requires an actin nucleation–promoting factor (NPF) to seed actin assembly (Goode *et al.*, 2001). In yeast, five endocytic NPFs have been identified: Pan1, Las17, Myo3, Myo5, and Abp1 (Winter *et al.*, 1999; Evangelista *et al.*, 2000; Lechler *et al.*, 2000; Duncan *et al.*, 2001; Goode *et al.*, 2001), although Pan1 and Abp1 are considered weak NPFs compared with the strong activities of Las17 or the type I myosins (Sun *et al.*, 2006). The WASp homologue, Las17, aids in recruitment of Vrp1, which in turn recruits and activates the redundant type I myosins Myo3 and Myo5 (Anderson *et al.*, 1998; Evangelista *et al.*, 2000; Geli *et al.*, 2000; Sirotkin *et al.*, 2005; Sun *et al.*, 2006; Wong *et al.*, 2010). Because verprolin binds these three potent NPFs, we tested whether *clc1-Δ19-76* would suppress null mutations in these genes.

The *clc1-Δ19-76* mutation was crossed to a *myo3*Δ *myo5*Δ strain, and resultant segregants were tested for growth. *myo3*Δ *myo5*Δ mutants showed extremely impaired growth at both 30 and 37°C, but combining the double null with *clc1-Δ19-76* suppressed this defect (Figure 7A). Again using time-lapse imaging, we examined Sla1, Sla2, and Abp1 for fluorescence lifetimes and movement (Figure 7, C, D, and G). In *myo3*Δ *myo5*Δ cells the lifetimes of Sla2 patches were extremely delayed compared with wild type, and only 8% of patches internalized, consistent with previous work (Sun *et al.*, 2006). However, these phenotypes were rescued by combination with the

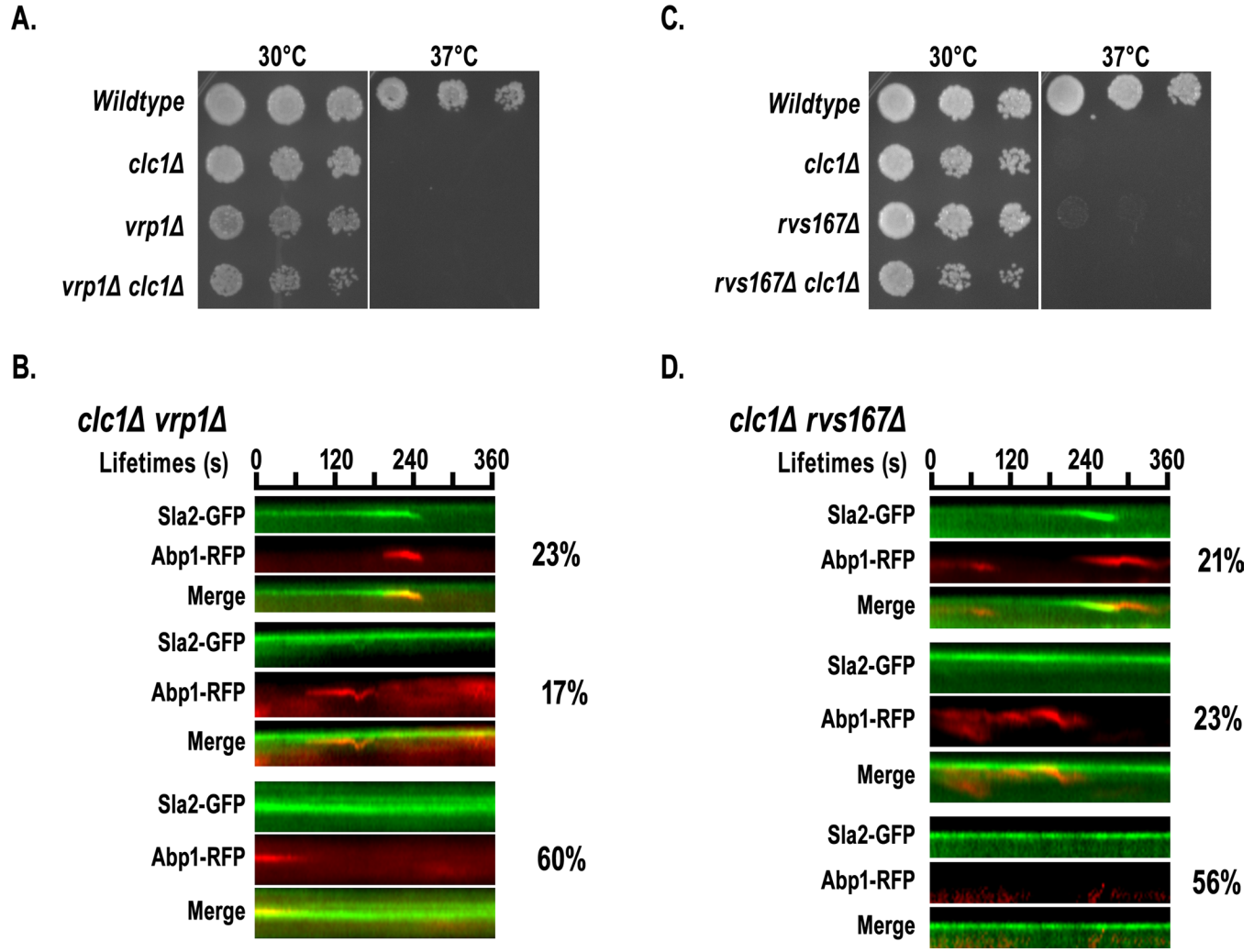


FIGURE 5: *vrp1*Δ and *rvs167*Δ are not suppressed by a clathrin LC null (*clc1*Δ). (A) Wild type (SL1462), *clc1*Δ (SL1620), *vrp1*Δ (SL4136), and *vrp1*Δ *clc1*Δ (SL6290) were fivefold serially diluted, plated on YEPD, and grown at 30 or 37°C for 60 h. (B) Kymographs of Sla2-GFP and Abp1-RFP in *vrp1*Δ *clc1*Δ (SL6291) illustrating the types of dynamic behaviors observed and percentages of each (n = 60). (C) Wild type (SL1462), *clc1*Δ (SL1620), *rvs167*Δ (RH2951), and *rvs167*Δ *clc1*Δ (SL6292) were plated and grown as indicated in A. (D) Kymographs of Sla2-GFP and Abp1-RFP in *rvs167*Δ *clc1*Δ (SL6293) illustrating the types of dynamic behaviors and percentages of each (n = 60).

*clc1-Δ19-76* allele. Sla2-GFP lifetimes decreased from 226 ± 102 to 56 ± 36 s ($p \leq 0.0001$, *myo3*Δ *myo5*Δ vs. *myo3*Δ *myo5*Δ *clc1-Δ19-76*, respectively; Figure 7, D and G), and the percentage of internalizing patches rose to 58% when *clc1-Δ19-76* was present in the myosin mutant. We also saw a mild effect of *clc1-Δ19-76* in *myo3*Δ (unpublished data) or *myo5*Δ alone (Figure 7, A and C–G), although generally the single myosin mutants were only slightly defective on their own, which explains why they did not appear in the SGA screen.

Deletion of *LAS17* caused temperature-sensitive growth at 37°C, which was also suppressed by *clc1-Δ19-76* (Figure 7B). *las17*Δ greatly increased both Sla1-GFP (80 ± 38 s), as shown previously (Sun *et al.*, 2006), and Sla2-GFP (124 ± 62 s) lifetimes compared with wild type (Figure 7, E–G). When *las17*Δ was combined with *clc1-Δ19-76* the lifetime of Sla1 was restored to normal (33 ± 7 s, $p \leq 0.0001$ vs. *las17*Δ), and there was significant improvement of the lifetime of Sla2 (78 ± 36 s, $p \leq 0.0001$ vs. *las17*Δ; Figure 7, E–G). Of interest, *clc1-Δ19-76* also suppressed the extended lifetime of Abp1-RFP in *las17*Δ or *myo3*Δ *myo5*Δ (Figure 7, C–G), which was not observed for *vrp1*Δ and *rvs167*Δ (Figures 3C and 4C). Overall these results show that *clc1-Δ19-76* also suppresses endocytic defects caused by loss of the major NPFs.

## DISCUSSION

In this study we performed SGA with yeast containing a deletion of the Sla2-binding region of CLC in order to elucidate the functional significance of this interaction in vivo. This unbiased approach identified a large number of negative genetic interactions with *clc1-Δ19-76*, including many with components involved in clathrin-mediated transport and TGN/endosomal trafficking. We focused on three endocytic factors, Vrp1, Rvs167, and Rvs161, whose mutations were suppressed by *clc1-Δ19-76*, as positive genetic interactions were likely to be specific to the *clc1-Δ19-76* allele and provide information on the regulatory role of the CLC–Sla2 interaction.

On the basis of our results, we propose the model shown in Figure 8, where CLC–Sla2 interaction prevents Sla2 binding to F-actin. This CLC inhibition would thereby restrict the number of attachments between Sla2 and actin, possibly to an area near the neck or edge of the clathrin coat (Figure 8A). Consistent with this,

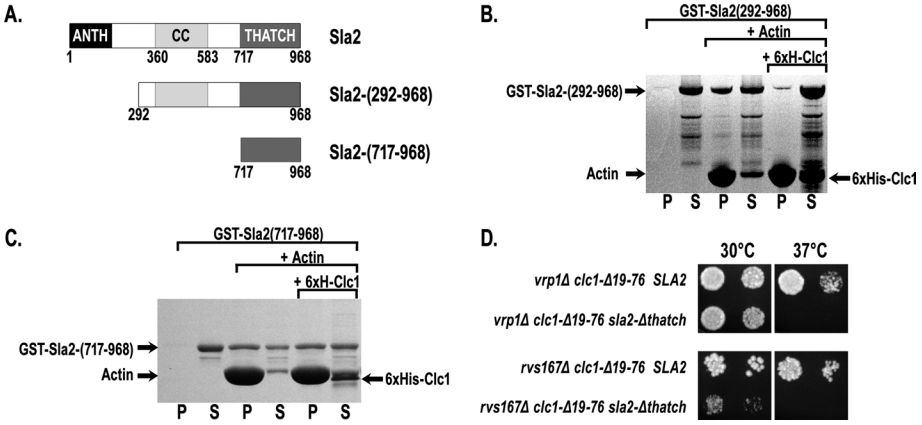


FIGURE 6: Clathrin LC inhibits Sla2 binding to F-actin. (A) GST-Sla2 fusions used in actin binding assays. Schematic highlights sequences corresponding to the N-terminal ANTH domain (black), coiled-coil domain (light gray), and THATCH domain (dark gray). (B) Actin sedimentation assays performed using 3 μM GST-Sla2-292-968, with or without 10 μM F-actin and with or without 15 μM 6xHis-Clc1. (C) Actin sedimentation assays performed as in B using 3 μM GST-Sla2-717-968.D. Sla2 actin-binding THATCH domain is necessary for *clc1-Δ19-76* suppression: strains were fivefold serially diluted, plated on YEPD, and grown at 30 and 37°C. Strains are *vrp1Δ clc1-Δ19-76* (SL6230), *vrp1Δ clc1-Δ19-76 sla2-Δthatch* (SL6231), *rvs167Δ clc1-Δ19-76* (SL6238), and *rvs167Δ clc1-Δ19-76 sla2-Δthatch* (SL6239).

immuno–electron microscopy (immuno-EM) of unroofed cells showed Hip1R associated with actin filaments primarily at the edge of clathrin lattices and pits (Engqvist-Goldstein *et al.*, 2001). In yeast Sla2–actin attachments at the edge of the pit may provide directionality to the force produced by actin assembly or even assist in vesicle scission. CLC is likely to achieve this regulation by causing conformational changes of Sla2 that regulate THATCH accessibility to actin. Self-interaction of the THATCH and coiled-coil regions of Sla2 were first suggested by two-hybrid analysis (Yang *et al.*, 1999). Electron microscopy of purified Hip1R or Hip1 showed the existence of both compact and extended profiles of the proteins (Engqvist-Goldstein *et al.*, 2001; Wilbur *et al.*, 2008), but the more compact structures are more prevalent in the presence of a 22–amino acid clathrin LCa N-terminal peptide containing the CLC-Hip1/R binding site (Wilbur *et al.*, 2008). Moreover, in surface plasmon resonance analysis the CLC NT peptide decreased the affinity of Hip1 or Hip1R binding to F-actin, suggesting that CLC binding in vitro negatively regulates Hip1/R attachments to actin by promoting Hip1/R self-interaction (Wilbur *et al.*, 2008).

Our work provides the first in vivo studies to support this regulatory model by showing that *clc1-Δ19-76*, a *clc1* mutant lacking its Sla2 interaction domain, can overcome several mutations leading to reduced late-stage actin assembly (*vrp1Δ*, *myo3Δ myo5Δ*, *las17Δ*) or failure to adequately narrow the neck of a vesicle (*rvs167Δ*/*rvs161Δ*). Recent studies suggested that CLC-NT prevents bending of the CHC knee, which impairs clathrin assembly (Wilbur *et al.*, 2010). Thus, deletion of the CLC-NT in our studies could be more favorable for formation of a curved lattice and promote membrane deformation. However, *clc1-Δ19-76* suppression of *vrp1Δ* and *rvs167Δ* depended on the actin-binding THATCH region of Sla2, which is more consistent with a mechanism of suppression involving Sla2 interaction with the actin cytoskeleton.

Immuno-EM analysis showed that the N-BAR proteins Rvs161 and Rvs167 are situated along the tubular invagination above the clathrin coat. This is consistent with their association with the narrowing neck of the invaginating vesicle and function in constriction of the membrane, leading to vesicle scission (Kaksonen *et al.*, 2005; Idrissi *et al.*, 2008). New studies suggest that the amphiphysins may work in concert with the yeast dynamin Vps1, although the endocytic defects of *vps1* mutants are much less severe and went unnoticed for some time (Nannapaneni *et al.*, 2010; Smaczynska-de *et al.*, 2010; our unpublished data). Although actin assembly would be robust in the amphiphysin mutants, the lack of constriction on the neck would impair scission, which is observed as retraction events by live-cell imaging (Kaksonen *et al.*, 2005; Smaczynska-de *et al.*, 2010; Youn *et al.*, 2010; Figure 8B). At the end of retraction, usually the coats and actin dissipate. We suggest that increased binding to actin by Sla2 allowed by the *clc1-Δ19-76* mutation might overcome this by stabilizing the coat and actin network (Figure 8D). This could drive the invaginations deeper into the cell, thus narrowing the neck of the invagination, or the new attachments could promote scission directly. Supporting this, in some cases we observed multiple retraction events and then internalization, as if the stabilization of the patch allowed added coat and actin assembly and new attempts at vesicle scission (D.R.B., unpublished observations).

The role of verprolin is to recruit and activate the type I myosins and is thus critical for the actin assembly burst that drives invagination (Anderson *et al.*, 1998; Geli *et al.*, 2000; Sirotkin *et al.*, 2005; Sun *et al.*, 2006). In yeast lacking Vrp1 (or myosin I function), there is no obvious inward movement of the endocytic coat (Figure 8C), despite the fact that the actin marker Abp1 is recruited (Sun *et al.*, 2006). Residual actin assembly is likely provided by other endocytic NPFs, including Las17 (WASp); however, these may not be sufficient or properly positioned to drive invagination when the myosin function is impaired. We suggest that this defect is overcome by *clc1-Δ19-76* since it would increase the duration of Sla2 binding to actin, as well as affect the location and number of attachments (Figure 8E). In addition, this may stabilize the actin network to overcome the reduced NPF activity caused by *vrp1Δ*'s effects on Myo3/5 activity.

Because *clc1-Δ19-76* could suppress *vrp1Δ*, one might predict that the *clc1-Δ19-76* allele could suppress other NPF mutations. Abp1 is a weak NPF, and *abp1Δ* has no phenotype on its own, so we did not expect to see suppression by the *clc1* mutation. However, our genetic screens found that *clc1-Δ19-76* exacerbated the growth defect of *pan1-4* (discussed later). We directly examined the three most potent NPF activities at the endocytic patch, Las17, and type I myosins (Winter *et al.*, 1999; Evangelista *et al.*, 2000; Lechler *et al.*, 2000; Duncan *et al.*, 2001; Goode *et al.*, 2001), which were not identified in the SGA screen. We found that *clc1-Δ19-76* also suppressed the growth and endocytic defects of l*as17Δ* and *myo3Δ myo5Δ*. Thus the model for verprolin (Figure 8) applies to these NPFs as well. Although *las17Δ* was not tested, three las17 *ts* alleles were analyzed by SGA, but their phenotypes may have been either too weak or too severe to observe suppression in a large-scale screen. Redundancy of the type-I myosins likely prevented their identification in the SGA.

We note that there was a difference in the suppression of *vrp1Δ* as compared with *las17Δ or myo3Δ myo5Δ*, in that *clc1-Δ19-76* suppressed the slowed Abp1 lifetime of these NPF mutations but not that of *vrp1Δ*. The reason for this distinction is not clear. Because Vrp1 binds both Las17 and the myosins, we suggest that Vrp1 also

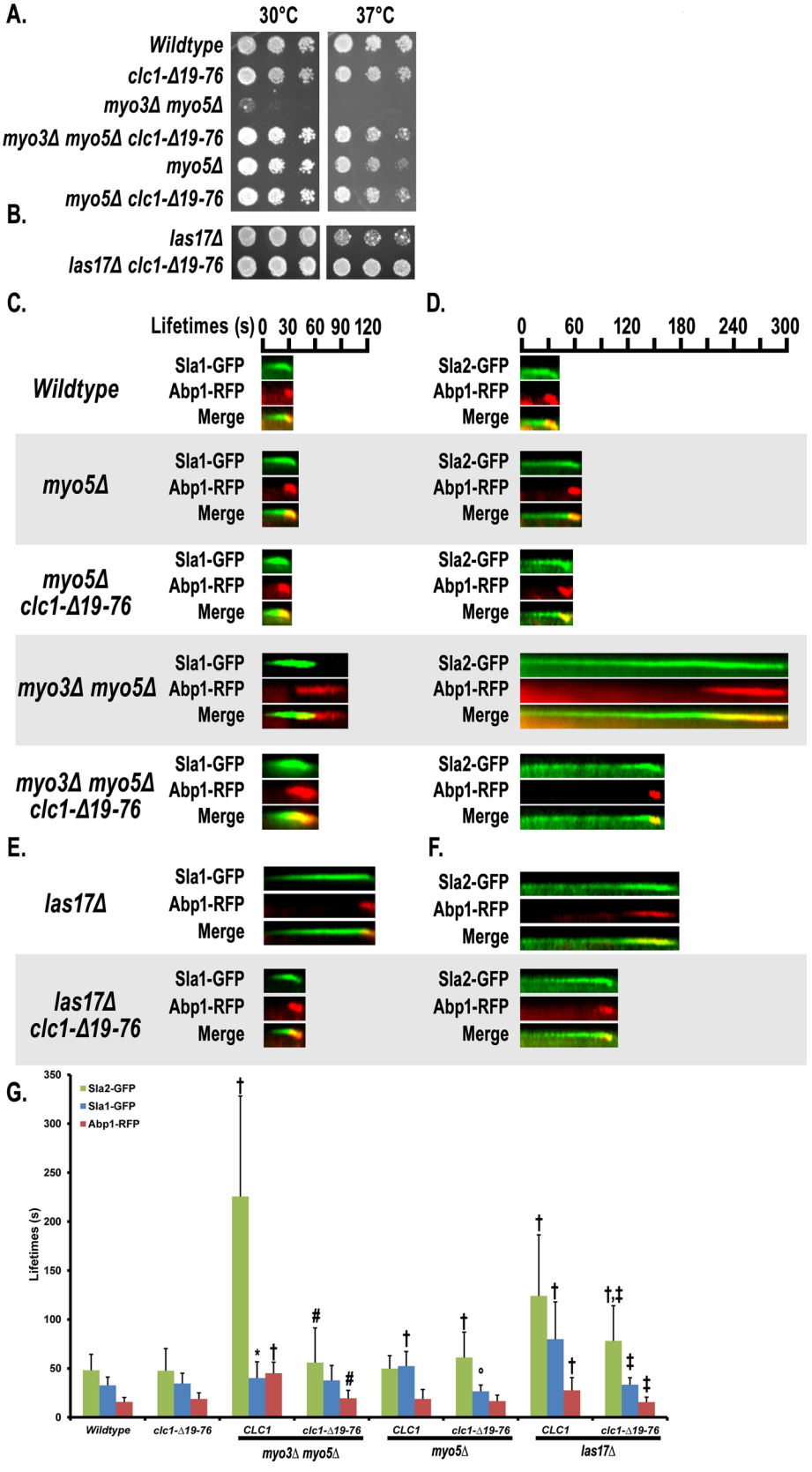


FIGURE 7: Endocytic defects caused by elimination of the type I myosins (*myo3Δ myo5Δ*) or WASp (*las17Δ*) are suppressed by *clc1-Δ19-76*. (A) Growth with *myo3Δ myo5Δ*: wild type (SL1462), *clc1-Δ19-76* (SL6044), *myo3Δ myo5Δ* (SL6561), *myo3Δ myo5Δ clc1-Δ19-76* (SL6576), *myo5Δ* (SL6580), and *myo5Δ clc1-Δ19-76* (SL6579) were fivefold serially diluted, plated on YEPD, and grown at 30 or 37°C for 60 h. (B) Growth of *las17Δ* (SL6602) and *las17Δ clc1-Δ19-76* (SL6603) as in A. (C) Representative kymographs of Sla1-GFP/Abp1-RFP patches in wild type (SL5311), *myo5Δ* (SL6579), *myo5Δ clc1-Δ19-76* (SL6554), *myo3Δ myo5Δ* (SL6562), and *myo3Δ myo5Δ clc1-Δ19-76* (SL6575). (D) Representative kymographs of Sla2-GFP/Abp1-RFP patches in wild type (SL5311), *myo5Δ* (SL6569), *myo5Δ clc1-Δ19-76* (SL6572), *myo5Δ myo3Δ* (SL6566), and *myo3Δ myo5Δ clc1-Δ19-76* (SL6568). (E) Representative kymographs of Sla1-GFP/Abp1-RFP patches in *las17Δ* (SL6596) and *las17Δ clc1-Δ19-76* (SL6597). (F) Representative kymographs of Sla2-GFP/Abp1-RFP patches in *las17Δ* (SL6598) and *las17Δ clc1-Δ19-76* (SL6600). (G) Fluorescence lifetimes of Sla2-GFP, Sla1-GFP, and Abp1-RFP in strains shown in C–F. Data are reported as average ± SD ($n \geq 50$). †$p \leq 0.0009$ vs. wild type; *$p \leq 0.004$ vs. wild type; #$p \leq 0.0001$ vs. *myo3Δ myo5Δ*; °$p \leq 0.0003$ vs. *myo5Δ*; ‡$p \leq 0.0001$ vs. *las17Δ*.

regulates the activity of the WASp. Thus in *vrp1Δ* the stimulatory activity of each of the major NPFs might be impaired, extending the time needed to produce a competent F-actin network for internalization. In *las17Δ or myo3Δ myo5Δ*, at least one of the major NPFs would still be active.

*PAN1* is one of the few essential endocytic genes. It encodes a scaffolding coat factor that binds several other endocytic coat proteins. Pan1 arrives at endocytic patches 20–30 s before the actin phase and has weak NPF activity (Kaksonen *et al.*, 2003; Sun *et al.*, 2006; Huang and Cai, 2007). In addition, the central domain of Sla2 (including the coiled-coil region) binds Pan1 and negatively regulates Pan1 NPF activity in vitro. Because the *pan1-4* product lacks its NPF activation domain (Li *et al.*, 2011), we initially surmised that the genetic interaction with *clc1-Δ19-76* might be due to Pan1's importance in priming actin assembly at the coat to initiate curvature. We tested this using *pan1-20*, which results in a truncation downstream of the NPF actin activation region but deletes the C-terminal proline-rich domain (PRD; Barker *et al.*, 2007). This mutant also caused synthetic lethality with *clc1-Δ19-76*, consistent with the *pan1-4* SGA results. These data suggest that the CLC-NT shares redundancy with functions of the Pan1-PRD, which may include the role of PRDs in binding to SH3-domain proteins (Barker *et al.*, 2007). However, we also cannot rule out that one role of CLC-NT binding to Sla2 may be to release Sla2's reported negative regulation of Pan1 NPF activity (Toshima *et al.*, 2007). The loss of CLC–Sla2 interaction might lead to prolonged Sla2 inhibition, which in the context of an impaired Pan1 could be

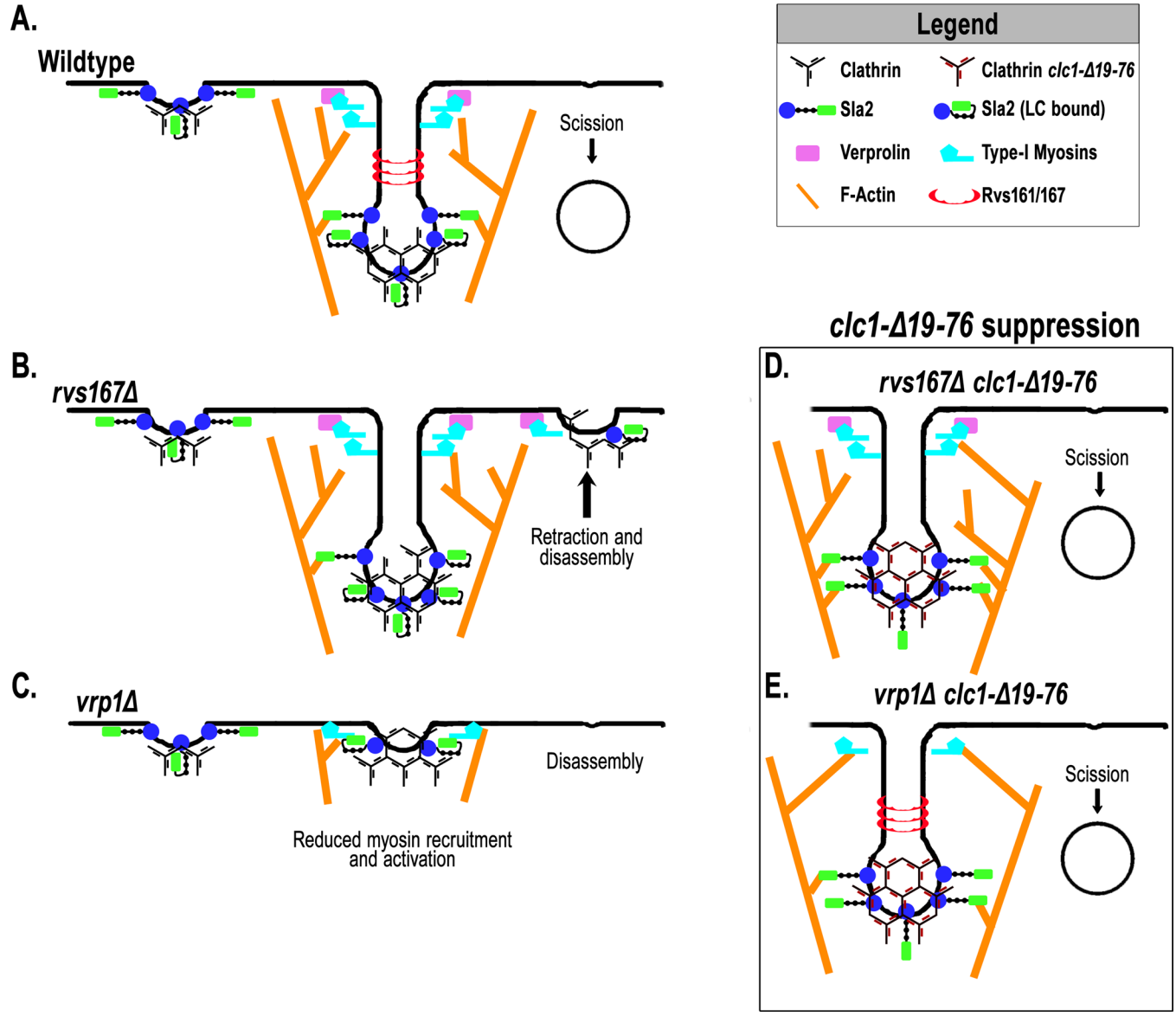


FIGURE 8: Model for CLC regulation of Sla2 binding to F-actin at endocytic patches. (A–C) Model of endocytic patches in wild type (A), *rvs167*Δ (B), and *vrp1*Δ (C). (D, E) Models for how preventing CLC regulation of the Sla2–actin interaction helps to overcome amphiphysin (D) and verprolin (E) mutants by increasing attachments to F-actin. Suppression of *myo3/5*Δ and *las17*Δ is similar to that of *vrp1*Δ.

severely detrimental. Further studies are needed to uncover the basis for this synthetic lethality.

In mammals, Hip1R binds F-actin barbed ends in association with cortactin, which inhibits actin filament depolymerization in vitro (Le Clainche *et al.*, 2007). This was suggested to channel new actin assembly and to stabilize F-actin. Despite a lack of a cortactin homologue in yeast, suppression by *clc1-Δ19-76* may involve a broader distribution of anchoring surrounding the invagination and increased stability of the network by barbed end binding. We note that capping protein also binds to barbed ends and terminates filament elongation, but Sla2 is unique in that its ANTH region would also serve to tether the membrane to actin. In fact, complete absence of Sla2 leads to impaired invagination and unproductive actin comet tails emanating from the cell surface (Kaksonen *et al.*, 2003). Thus, localized Sla2 contact with F-actin performs a unique function in directing elongation of the membrane protrusions and/or scission.

The invaginating sites in yeast have an extended tubular morphology with a clathrin coat at the tip and actin assembled surrounding the tubule (Idrissi *et al.*, 2008). This architecture of such tubular assemblies with associated actin and clathrin has also been observed in mammalian cells. For example, internalizing vesicular stomatitis virus was found in deep invagination profiles with a clathrin cap at its base and an extensive actin network along the membrane surrounding the virus extending up to the cell surface, suggesting that actin is required for clathrin-mediated endocytosis of large particles (Cureton *et al.*, 2009). In addition, long actin-dependent tubules with clathrin pits at the tip are generated in dynamin 1 and 2 double-knockout cells (Ferguson *et al.*, 2009). These endocytic structures have been recapitulated in vitro from plasma membrane sheets incubated in the presence of cytosol and GTPγS, which blocks scission (Wu *et al.*, 2010). Although the manner in which these structures are formed is unknown, they share remarkable

similarities with yeast tubular invaginations, suggesting a role for Hip1 and Hip1R in their formation.

In summary, we believe that our results support the idea that a major role of CLC is to control endocytic progression by pruning the Sla2–actin attachments in the endocytic coat so that anchoring is restricted, possibly to the edge or neck of the invaginating vesicle. Releasing attachments in the coat could contribute to development of the endocytic vesicle and may be needed to promote directional membrane internalization. Restricting attachments to near the neck might also promote vesicle scission.

## MATERIALS AND METHODS

### Yeast strains and growth assays

*Saccharomyces cerevisiae* strains used in this study are listed in Supplemental Table S1A. Standard methods and media were used for genetic manipulations, growth, and transformation of yeast (Guthrie and Fink, 1991). To perform growth-plating assays, overnight log-phase liquid cultures were diluted to a starting concentration of $5 \times 10^6$ cells/ml and then fivefold serially diluted in 96-well plates. Diluted cells were pinned with a multiprong frog onto yeast extract/peptone/dextrose (YEPD) plates and grown at indicated temperatures for 48–60 h.

Generation of the integrated clathrin light-chain allele (*clc1-Δ19-76:NatMX6*) was done as follows. First a HisMX6 PCR fragment, flanked by *Nco*1 sites with *CLC1* ends to excise codons 19–76, was cotransformed into yeast with pRS424 containing *CLC1*. Recombinant plasmids were shuttled into bacteria from Trp+ His+ colonies, cut with *Nco*1, and ligated to excise the *HisMX6*, yielding pTM45 with the *clc1-Δ19-76* allele. Note that the religation changed codon 19 from GAC (Asp) to GAA (Glu) and inserted two codons representing the *Nco*I site: CCA (Pro) and TGG (Trp). Next the NatMX6 marker was PCR amplified from a pFA6a-NatMX6 template and integrated via homologous recombination downstream of the *clc1-Δ19-76* coding sequence in pTM45. The resultant plasmid (pDRB1) was used as a template for two PCR amplifications. The first contained the 5′ flanking *CLC1* DNA, the mutant allele, and 500 nucleotides of the NatMX6 marker. The second contained the full NatMX6 marker followed by 3′ sequence flanking *CLC1*. These products were cotransformed into the SGA tester strain y7092 (Tong *et al.*, 2007), as well as our laboratory wild-type strain (SL1462) for split marker recombination (Catlett *et al.*, 2003), and screened for simultaneous recombination at the *CLC1* locus, generating SL5677 and SL6044, respectively. The integrated mutant alleles were recovered by PCR and confirmed by DNA sequencing.

The integrated *SLA2-GFP:TRP1* was generated by homologous recombination as previously described (Wach *et al.*, 1997; Longtine *et al.*, 1998), using pFA6a-*TRP1* as a template. Similarly, *SLA2-HA:HisMX6* and *SLA2-ΔTHATCH-HA:HisMX6* were generated using pFA6a-3HA-HisMX6 as the template. The coding sequence for the HA tag in *SLA2-ΔTHATCH-HA:HisMX6* was integrated after *SLA2* codon 716. Strains for endocytic factor lifetimes and phenotypic analyses were created by standard genetic crosses. To avoid problems of polyploidy found in clathrin-null strains, haploid *clc1Δ:HIS3* spores that segregated from tetrads with pKH2 (*CLC1*, 2 μ, *URA3*) (Huang *et al.*, 1997) were used in crosses. Diploids were selected, grown on 5-fluoroorotic acid to drop the *CLC1* plasmid, and then sporulated and dissected.

### SGA screens

SGA screens were conducted as described (Tong and Boone, 2006). In one screen the *clc1-Δ19-76:NatMX6* query strain (SL5677) was crossed to a miniarray consisting of 177 strains with *ts* mutations in genes annotated with roles in actin, endocytosis, and vesicle trafficking (www.yeastgenome.org; Supplemental Table S1B). Construction of the *ts* mutant strains and methodology for screening them have been described (Li *et al.*, 2011). The second screen was performed against an array of 3885 nonessential null mutants. Genetic interactions from the SGA screens were processed and identified as previously described (Tong *et al.*, 2004). The results from the knockout screen were normalized and the interactions measured as deviations from the null mutant alone. These relative fitness measurements were used to assign genetic interaction scores ε as described in Costanzo *et al.* (2010). Results here are reported as synthetic rescue if they had $\varepsilon > 0.16$ and $p < 0.05$. Results are reported as synthetic growth defects if they had $\varepsilon < -0.12$ and $p < 0.05$.

Assignment of screen results to biological process (Supplemental Table S2) was performed based on Gene Ontology assignments using Slim-Go enrichment at the *Saccharomyces* Genome Database (www.yeastgenome.org) and then manually refined. To perform network analysis, each screen hit was used as a node, and additional node/edge attributes (from the *Saccharomyces* Genome Database) were layered onto the data set using Cytoscape (Kohl *et al.*, 2010). Known physical interactions were used to identify protein complexes (Figures 1, D–G) using the MCODE plug-in for Cytoscape (Bader and Hogue, 2003).

### Microscopy and image analysis

Live-cell imaging of endocytosis was carried out essentially as described in Boettner *et al.* (2009). Cells were grown to log phase at 25°C in synthetic medium, concentrated, immobilized on polylysine-coated coverslips, mounted on slides in 1.6% agarose, and then imaged at 25°C. All fluorescence lifetimes were calculated from movies acquired on an Olympus (Center Valley, PA) BX71 inverted microscope equipped with differential interference contrast (DIC) optics, an UPlan Apo 150× total internal reflection fluorescence objective (numerical aperture [NA], 1.45), Hamamatsu (Hamamatsu, Japan) ImagEM C910013 512 × 512 bit EM charge-coupled device camera, and a Sutter Instrument (Novato, CA) Lambda DG4 rapid wavelength switcher with a 300-W xenon lamp. Images were captured using SlideBook 4.2 for PC platform (Intelligent Imaging Innovations, Denver, CO). Following capture, all movies were photobleach corrected in SlideBook using the exponential correction function. Average patch lifetimes and standard deviations were determined from 30–40 patches for each strain. Student's *t* test was used to calculate p values. All kymographs, projection images, and example micrographs were generated in SlideBook and then exported to Adobe Photoshop (San Jose, CA) for figure assembly.

Single-particle tracks were generated from movies exported from SlideBook into ImageJ (National Institutes of Health, Bethesda, MD) using the plug-in ParticleTracker (Sbalzarini and Koumoutsakos, 2005). Particle trajectories that aligned 90 deg from the cell cortex were converted from pixel to metric distances and graphed using SigmaPlot.

All other microscopy was carried out on an Olympus fluorescence BX61 upright microscope equipped with Nomarski DIC optics, a UPlan S Apo 100× objective (NA 1.4), a CoolSnap HQ camera (Roper Scientific Germany, Ottobrunn, Germany), Sutter Instrument Lambda 10-2 excitation and emission filter wheels, and a 175-W xenon remote source with liquid light guide. Image capture was automated using SlideBook 4.01 for the Mac.

Analysis of actin polarization in phalloidin stained cells was done as follows. Cells were grown in YEPD to a concentration of $5 \times 10^6$ cells/ml at 30°C. Formaldehyde was added directly to growth medium to a final concentration of 4%, and cultures were continued for

10 min. Cells were collected and resuspended in phosphate-buffered saline (PBS; 140 mM NaCl, 2.7 mM KCl, 10 mM $Na_2HPO_4$, 1.8 mM $KH_2PO_4$) containing 4% formaldehyde and incubated at room temperature for an additional 1 h. After two washes in PBS, cells were stained overnight at 4°C with 6.6 μM Alexa 568–phalloidin (Molecular Probes, Invitrogen, Carlsbad, CA). Cells were washed five times in PBS and immobilized on polylysine-coated coverslips for imaging. A series of optical Z-sections (0.2 μm) ware captured and then deconvolved by the nearest-neighbor algorithm and projected into a single plane using SlideBook. Polarization of actin was quantified on cells with small or medium-size buds as described by Bi *et al*. (1998). Total fluorescence measurements were made for the whole cell and the mother cell in SlideBook. Cells with more than 50% of the total fluorescence in the mother cell were scored as nonpolarized (n = 50).

Lucifer yellow (Molecular Probes) uptake was performed at 30°C for 1 h as described in Dulic *et al*. (1991).

### Biochemical methods

Bacterial expression plasmids for GST-Sla2 (pTMN5), GST-Sla2-(292-968), and 6xHis-Clc1 (pTMN3) are described in Newpher and Lemmon (2006). GST-Crn1 was expressed in bacteria from pGAT2-CRN(1–651) (Goode *et al*., 1999). The vector for expression of GST-Sla2-(717-968) (pDRB7) was generated by ligation of a *SLA2* PCR fragment encoding amino acids 717–968 (THATCH domain) with *Bam*H1/*Sal*1 ends into pGEX-4t.

GST fusions were expressed in Rosetta *Escherichia coli* (Agilent Technologies, Santa Clara, CA). Cultures were grown to log phase at 37°C, then induced with 0.5 mM isopropyl-β-D-thiogalactoside for 6 h at 25°C. After pelleting, cells were resuspended in lysis buffer (140 mM NaCl, 2.7 mM KCl, 10 mM $Na_2HPO_4$, 1.8 mM $KH_2PO_4$, pH 7.3) containing 0.5% Triton X-100 (v/v), 1 mM dithiothreitol (DTT), a protease inhibitor cocktail (Stepp *et al*., 1995), and lysozyme (0.5 mg/ml) and incubated on ice for 15 min. Cells were lysed by sonication, and the lysate was cleared by centrifugation at 16,000 × *g* for 20 min. GST fusions were absorbed from the cleared supernatant onto glutathione–agarose beads (GE Healthcare, Piscataway, NJ) for 1.5 h on a rocker at 4°C. Beads were loaded into a poly-prep chromatography column (0.8 × 4 cm; Bio-Rad, Hercules, CA) and washed in 10 column volumes of lysis buffer, and then GST fusions were eluted in 50 mM Tris-HCl, pH 8.0, 10 mM reduced glutathione, and 1 mM DTT. Peak fractions were exchanged into actin assembly buffer (see later discussion), concentrated in a Centricon-10 size exclusion filter (Millipore, Billerica, MA), brought up to 10% glycerol, snap frozen, and stored at −80°C. The 6xHis-Clc1 (pTMN3) was expressed and purified from BL-21 *E. coli* (DE3) as described in Newpher and Lemmon (2006).

Actin cosedimentation assays were performed as described by Gohla *et al*. (2005). Prior to use, all protein samples proteins were precleared by centrifugation at 100,000 × *g* in a Beckman Airfuge equipped with an A-100 rotor. Nonmuscle actin (Cytoskeleton, Denver, CO) was assembled for 1 h at room temperature in actin assembly buffer (4.5 mM Tris-HCl, 20 μM $CaCl_2$, 50 mM KCl, 2 mM $MgCl_2$, 1 mM ATP, pH 8.0). Assembled F-actin was added at a final concentration of 10 μM to either input proteins alone or input proteins preincubated for 1 h with a fivefold molar excess of 6xHis-Clc1. Input proteins were tested at the following concentrations: 3 μM GST-Sla2-292-958, 3 μM GST-Sla2-717-968, 1 μM GST-Sla2, and 1 μM GST-Crn1. Binding reactions were performed at 25°C for 1 h (typically in 50 μl ) in actin assembly buffer, and then actin and actin-associated proteins were pelleted by centrifugation in the Airfuge at 100,000 × *g* for 1 h at room temperature. The supernatant was removed and the pellet was resuspended in water. The supernatant and pellet were brought to equal volumes in SDS–PAGE loading buffer, boiled for 3 min, and separated by SDS–PAGE on 8–20% gradient polyacrylamide gels (Invitrogen). Gels were stained with Coomassie brilliant blue, and high-resolution images were captured for densitometry analysis using ImageJ. Trapping of soluble proteins was accounted for by sedimentation of bovine serum albumin (2 μM) in the presence of 10 μM F-actin.

For immunoblots of clathrin LC and HC, cultures were grown to log phase ($5 \times 10^6$ cells/ml) at 30°C, and 10 ml were concentrated and subjected to glass bead lysis in 250 μl of 0.1 M Tris, pH 7.5, containing 1 mM phenylmethylsulfonyl fluoride and a protease inhibitor cocktail (Stepp *et al*., 1995). Lysates were centrifuged for 20 min at 10,000 × *g*, and equivalent volumes of the supernatants were analyzed by SDS–PAGE and immunoblotted using anti-Chc1 mouse monoclonal antibodies (Lemmon *et al*., 1988), anti-Clc1 rabbit polyclonal antiserum (a gift from Greg Payne), or anti-PGK1 mouse monoclonal antibodies (Molecular Probes) as a loading control. Antibody decoration was detected by an Odyssey Infrared Imaging System (LiCor, Lincoln, NE) using IRDye700- or IRDye800-conjugated secondary antiserum (LiCor).

## ACKNOWLEDGMENTS

We thank Howard Riezman, Anita Hopper, Mark Rose, Greg Payne, Bruce Goode, Beverly Wendland, and Maribel Geli for providing strains, reagents, and constructs. We are also very grateful to James Potter and Michelle Jones for providing purified actin for our initial studies. D.R.B. was supported by a National Institutes of Health National Research Service Awards Fellowship (F32-GM084677). This work was funded by National Institutes of Health Grants R01-GM055796 (S.K.L.) and R01-HG005853 (B.A.).

## REFERENCES

Anderson BL, Boldogh I, Evangelista M, Boone C, Greene LA, Pon LA (1998). The Src homology domain 3 (SH3) of a yeast type I myosin, Myo5p, binds to verprolin and is required for targeting to sites of actin polarization. J Cell Biol 141, 1357–1370.

Bader GD, Hogue CW (2003). An automated method for finding molecular complexes in large protein interaction networks. BMC Bioinformatics 4, 2.

Barker SL, Lee L, Pierce BD, Maldonado-Baez L, Drubin DG, Wendland B (2007). Interaction of the endocytic scaffold protein Pan1 with the type I myosins contributes to the late stages of endocytosis. Mol Biol Cell 18, 2893–2903.

Bensen ES, Costaguta G, Payne GS (2000). Synthetic genetic interactions with temperature-sensitive clathrin in *Saccharomyces cerevisiae*. Roles for synaptojanin-like Inp53p and dynamin-related Vps1p in clathrin-dependent protein sorting at the trans-Golgi network. Genetics 154, 83–97.

Bensen ES, Yeung BG, Payne GS (2001). Ric1p and the Ypt6p GTPase function in a common pathway required for localization of trans-Golgi network membrane proteins. Mol Biol Cell 12, 13–26.

Bi E, Maddox P, Lew DJ, Salmon ED, McMillan JN, Yeh E, Pringle JR (1998). Involvement of an actomyosin contractile ring in *Saccharomyces cerevisiae* cytokinesis. J Cell Biol 142, 1301–1312.

Boettner DR, D'Agostino JL, Torres OT, Daugherty-Clarke K, Uygur A, Reider A, Wendland B, Lemmon SK, Goode BL (2009). The F-BAR protein Syp1 negatively regulates WASp-Arp2/3 complex activity during endocytic patch formation. Curr Biol 19, 1979–1987.

Boldogh IR, Yang HC, Nowakowski WD, Karmon SL, Hays LG, Yates JR 3rd, Pon LA (2001). Arp2/3 complex and actin dynamics are required for actin-based mitochondrial motility in yeast. Proc Natl Acad Sci USA 98, 3162–3167.

Brett TJ, Legendre-Guillemin V, McPherson PS, Fremont DH (2006). Structural definition of the F-actin-binding THATCH domain from HIP1R. Nat Struct Mol Biol 13, 121–130.

Catlett NL, Lee B-N, Yoder OC, Turgeon BG (2003). Split-marker recombination for efficient targeted deletion of fungal genes. Fungal Genet News 50, 9–11.

Chen CY, Brodsky FM (2005). Huntingtin-interacting protein 1 (Hip1) and Hip1-related protein (Hip1R) bind the conserved sequence of clathrin light chains and thereby influence clathrin assembly in vitro and actin distribution in vivo. J Biol Chem 280, 6109–6117.

Chu DS, Pishvaee B, Payne GS (1996). The light chain subunit is required for clathrin function in *Saccharomyces cerevisiae*. J Biol Chem 271, 33123–33130.

Costanzo M *et al*. (2010). The genetic landscape of a cell. Science 327, 425–431.

Cureton DK, Massol RH, Saffarian S, Kirchhausen TL, Whelan SP (2009). Vesicular stomatitis virus enters cells through vesicles incompletely coated with clathrin that depend upon actin for internalization. PLoS Pathog 5, e1000394.

Dulic V, Egerton M, Elguindi I, Raths S, Singer B, Riezman H (1991). Yeast endocytosis assays. Methods Enzymol 194, 697–710.

Duncan MC, Cope MJ, Goode BL, Wendland B, Drubin DG (2001). Yeast Eps15-like endocytic protein, Pan1p, activates the Arp2/3 complex. Nat Cell Biol 3, 687–690.

Engqvist-Goldstein AE, Drubin DG (2003). Actin assembly and endocytosis: from yeast to mammals. Annu Rev Cell Dev Biol 19, 287–332.

Engqvist-Goldstein AE, Warren RA, Kessels MM, Keen JH, Heuser J, Drubin DG (2001). The actin-binding protein Hip1R associates with clathrin during early stages of endocytosis and promotes clathrin assembly in vitro. J Cell Biol 154, 1209–1223.

Engqvist-Goldstein AE, Zhang CX, Carreno S, Barroso C, Heuser JE, Drubin DG (2004). RNAi-mediated Hip1R silencing results in stable association between the endocytic machinery and the actin assembly machinery. Mol Biol Cell 15, 1666–1679.

Evangelista M, Klebl BM, Tong AH, Webb BA, Leeuw T, Leberer E, Whiteway M, Thomas DY, Boone C (2000). A role for myosin-I in actin assembly through interactions with Vrp1p, Bee1p, and the Arp2/3 complex. J Cell Biol 148, 353–362.

Ferguson SM *et al*. (2009). Coordinated actions of actin and BAR proteins upstream of dynamin at endocytic clathrin-coated pits. Dev Cell 17, 811–822.

Fotin A, Cheng Y, Sliz P, Grigorieff N, Harrison SC, Kirchhausen T, Walz T (2004). Molecular model for a complete clathrin lattice from electron cryomicroscopy. Nature 432, 573–579.

Friesen H, Humphries C, Ho Y, Schub O, Colwill K, Andrews B (2006). Characterization of the yeast amphiphysins Rvs161p and Rvs167p reveals roles for the Rvs heterodimer in vivo. Mol Biol Cell 17, 1306–1321.

Galletta BJ, Chuang DY, Cooper JA (2008). Distinct roles for Arp2/3 regulators in actin assembly and endocytosis. PLoS Biol 6, e1.

Galletta BJ, Mooren OL, Cooper JA (2010). Actin dynamics and endocytosis in yeast and mammals. Curr Opin Biotechnol 21, 604–610.

Geli MI, Lombardi R, Schmelzl B, Riezman H (2000). An intact SH3 domain is required for myosin I-induced actin polymerization. EMBO J 19, 4281–4291.

Gohla A, Birkenfeld J, Bokoch GM (2005). Chronophin, a novel HAD-type serine protein phosphatase, regulates cofilin-dependent actin dynamics. Nat Cell Biol 7, 21–29.

Goode BL, Rodal AA (2001). Modular complexes that regulate actin assembly in budding yeast. Curr Opin Microbiol 4, 703–712.

Goode BL, Rodal AA, Barnes G, Drubin DG (2001). Activation of the Arp2/3 complex by the actin filament binding protein Abp1p. J Cell Biol 153, 627–634.

Goode BL, Wong JJ, Butty AC, Peter M, McCormack AL, Yates JR, Drubin DG, Barnes G (1999). Coronin promotes the rapid assembly and cross-linking of actin filaments and may link the actin and microtubule cytoskeletons in yeast. J Cell Biol 144, 83–98.

Guthrie C, Fink GR (1991). Guide to yeast genetics and molecular biology. Methods Enzymol 194, 1–933.

Henry KR, D'Hondt K, Chang J, Newpher T, Huang K, Hudson RT, Riezman H, Lemmon SK (2002). Scd5p and clathrin function are important for cortical actin organization, endocytosis, and localization of Sla2p in yeast. Mol Biol Cell 13, 2607–2625.

Huang B, Cai M (2007). Pan1p: an actin director of endocytosis in yeast. Int J Biochem Cell Biol 39, 1760–1764.

Huang F, Khvorova A, Marshall W, Sorkin A (2004). Analysis of clathrin-mediated endocytosis of epidermal growth factor receptor by RNA interference. J Biol Chem 279, 16657–16661.

Huang KM, Gullberg L, Nelson KK, Stefan CJ, Blumer K, Lemmon SK (1997). Novel functions of clathrin light chains: clathrin heavy chain trimerization is defective in light chain-deficient yeast. J Cell Sci 110, 899–910.

Hyun TS, Rao DS, Saint-Dic D, Michael LE, Kumar PD, Bradley SV, Mizukami IF, Oravecz-Wilson KI, Ross TS (2004). HIP1 and HIP1r stabilize receptor tyrosine kinases and bind 3-phosphoinositides via epsin N-terminal homology domains. J Biol Chem 279, 14294–14306.

Idrissi FZ, Grotsch H, Fernandez-Golbano IM, Presciatto-Baschong C, Riezman H, Geli MI (2008). Distinct acto/myosin-I structures associate with endocytic profiles at the plasma membrane. J Cell Biol 180, 1219–1232.

Jonsdottir GA, Li R (2004). Dynamics of yeast myosin I: evidence for a possible role in scission of endocytic vesicles. Curr Biol 14, 1604–1609.

Kaksonen M, Sun Y, Drubin DG (2003). A pathway for association of receptors, adaptors, and actin during endocytic internalization. Cell 115, 475–487.

Kaksonen M, Toret CP, Drubin DG (2005). A modular design for the clathrin- and actin-mediated endocytosis machinery. Cell 123, 305–320.

Kohl M, Wiese S, Warscheid B (2010). Cytoscape: software for visualization and analysis of biological networks. Methods Mol Biol 696, 291–303.

Le Clainche C, Pauly BS, Zhang CX, Engqvist-Goldstein AE, Cunningham K, Drubin DG (2007). A Hip1R-cortactin complex negatively regulates actin assembly associated with endocytosis. EMBO J 26, 1199–1210.

Lechler T, Shevchenko A, Li R (2000). Direct involvement of yeast type I myosins in Cdc42-dependent actin polymerization. J Cell Biol 148, 363–373.

Legendre-Guillemin V, Metzler M, Charbonneau M, Gan L, Chopra V, Philie J, Hayden MR, McPherson PS (2002). HIP1 and HIP12 display differential binding to F-actin, AP2, and clathrin. Identification of a novel interaction with clathrin light chain. J Biol Chem 277, 19897–19904.

Legendre-Guillemin V, Metzler M, Lemaire JF, Philie J, Gan L, Hayden MR, McPherson PS (2005). Huntingtin interacting protein 1 (HIP1) regulates clathrin assembly through direct binding to the regulatory region of the clathrin light chain. J Biol Chem 280, 6101–6108.

Lemmon S, Lemmon VP, Jones EW (1988). Characterization of yeast clathrin and anticlathrin heavy-chain monoclonal antibodies. J Cell Biochem 36, 329–340.

Lemmon SK, Freund C, Conley K, Jones EW (1990). Genetic instability of clathrin-deficient strains of *Saccharomyces cerevisiae*. Genetics 124, 27–38.

Li Z *et al*. (2011). Systematic exploration of essential yeast gene function with temperature-sensitive mutants. Nat Biotechnol 29, 361–367.

Liu SH, Wong ML, Craik CS, Brodsky FM (1995). Regulation of clathrin assembly and trimerization defined using recombinant triskelion hubs. Cell 83, 257–267.

Lombardi R, Riezman H (2001). Rvs161p and Rvs167p, the two yeast amphiphysin homologs, function together in vivo. J Biol Chem 276, 6016–6022.

Longtine MS, McKenzie A 3rd, Demarini DJ, Shah NG, Wach A, Brachat A, Philippsen P, Pringle JR (1998). Additional modules for versatile and economical PCR-based gene deletion and modification in *Saccharomyces cerevisiae*. Yeast 14, 953–961.

McCann RO, Craig SW (1997). The I/LWEQ module: a conserved sequence that signifies F-actin binding in functionally diverse proteins from yeast to mammals. Proc Natl Acad Sci USA 94, 5679–5684.

Munn AL, Stevenson BJ, Geli MI, Riezman H (1995). *end5*, *end6*, and *end7*: mutations that cause actin delocalization and block the internalization step of endocytosis in *Saccharomyces cerevisiae*. Mol Biol Cell 6, 1721–1742.

Nannapaneni S *et al*. (2010). The yeast dynamin-like protein Vps1: *vps1* mutations perturb the internalization and the motility of endocytic vesicles and endosomes via disorganization of the actin cytoskeleton. Eur J Cell Biol 89, 499–508.

Nelson KK, Lemmon SK (1993). Suppressors of clathrin deficiency: overexpression of ubiquitin rescues lethal strains of clathrin-deficient *Saccharomyces cerevisiae*. Mol Cell Biol 13, 521–532.

Newpher TM, Idrissi FZ, Geli MI, Lemmon SK (2006). Novel function of clathrin light chain in promoting endocytic vesicle formation. Mol Biol Cell 17, 4343–4352.

Newpher TM, Lemmon SK (2006). Clathrin is important for normal actin dynamics and progression of Sla2p-containing patches during endocytosis in yeast. Traffic 7, 574–588.

Newpher TM, Smith RP, Lemmon V, Lemmon SK (2005). In vivo dynamics of clathrin and its adaptor-dependent recruitment to the actin-based endocytic machinery in yeast. Dev Cell 9, 87–98.

Poupon V, Girard M, Legendre-Guillemin V, Thomas S, Bourbonniere L, Philie J, Bright NA, McPherson PS (2008). Clathrin light chains function in mannose phosphate receptor trafficking via regulation of actin assembly. Proc Natl Acad Sci USA 105, 168–173.

Reider A, Barker SL, Mishra SK, Im YJ, Maldonado-Baez L, Hurley JH, Traub LM, Wendland B (2009). Syp1 is a conserved endocytic adaptor that contains domains involved in cargo selection and membrane tubulation. EMBO J 28, 3103–3116.

Robertson AS, Smythe E, Ayscough KR (2009). Functions of actin in endocytosis. Cell Mol Life Sci 66, 2049–2065.

Saffarian S, Cocucci E, Kirchhausen T (2009). Distinct dynamics of endocytic clathrin-coated pits and coated plaques. PLoS Biol 7, e1000191.

Sbalzarini IF, Koumoutsakos P (2005). Feature point tracking and trajectory analysis for video imaging in cell biology. J Struct Biol 151, 182–195.

Senetar MA, Foster SJ, McCann RO (2004). Intrasteric inhibition mediates the interaction of the I/LWEQ module proteins Talin1, Talin2, Hip1, and Hip12 with actin. Biochemistry 43, 15418–15428.

Simpson PJ, Schwappach B, Dohlman HG, Isaacson RL (2010). Structures of Get3, Get4, and Get5 provide new models for TA membrane protein targeting. Structure 18, 897–902.

Sirotkin V, Beltzner CC, Marchand JB, Pollard TD (2005). Interactions of WASp, myosin-I, and verprolin with Arp2/3 complex during actin patch assembly in fission yeast. J Cell Biol 170, 637–648.

Smaczynska-de R II, Allwood EG, Aghamohammadzadeh S, Hettema EH, Goldberg MW, Ayscough KR (2010). A role for the dynamin-like protein Vps1 during endocytosis in yeast. J Cell Sci 123, 3496–3506.

Stepp JD, Pellicena-Palle A, Hamilton S, Kirchhausen T, Lemmon SK (1995). A late Golgi sorting function for *Saccharomyces cerevisiae* Apm1p, but not for Apm2p, a second yeast clathrin AP medium chain-related protein. Mol Biol Cell 6, 41–58.

Stimpson HE, Toret CP, Cheng AT, Pauly BS, Drubin DG (2009). Early-arriving Syp1p and Ede1p function in endocytic site placement and formation in budding yeast. Mol Biol Cell 20, 4640–4651.

Sun Y, Kaksonen M, Madden DT, Schekman R, Drubin DG (2005). Interaction of Sla2p's ANTH domain with PtdIns(4,5)P2 is important for actin-dependent endocytic internalization. Mol Biol Cell 16, 717–730.

Sun Y, Martin AC, Drubin DG (2006). Endocytic internalization in budding yeast requires coordinated actin nucleation and myosin motor activity. Dev Cell 11, 33–46.

Tong AH, Boone C (2006). Synthetic genetic array analysis in *Saccharomyces cerevisiae*. Methods Mol Biol 313, 171–192.

Tong AH *et al*. (2004). Global mapping of the yeast genetic interaction network. Science 303, 808–813.

Tong AHY, Boone C, Ian S, Michael JRS (2007). High-throughput strain construction and systematic synthetic lethal screening in *Saccharomyces cerevisiae*. In: Methods in Microbiology, Volume 36, I Stansfield and MJR Stark, London: Academic Press, 369–386.

Toshima J, Toshima JY, Duncan MC, Cope MJ, Sun Y, Martin AC, Anderson S, Yates JR 3rd, Mizuno K, Drubin DG (2007). Negative regulation of yeast Eps15-like Arp2/3 complex activator, Pan1p, by the Hip1R-related protein, Sla2p, during endocytosis. Mol Biol Cell 18, 658–668.

Traub LM (2005). Common principles in clathrin-mediated sorting at the Golgi and the plasma membrane. Biochim Biophys Acta 1744, 415–437.

Ungewickell E, Ungewickell H (1991). Bovine brain clathrin light chains impede heavy chain assembly in vitro. J Biol Chem 266, 12710–12714.

Wach A, Brachat A, Alberti-Segui C, Rebischung C, Philippsen P (1997). Heterologous *HIS3* marker and GFP reporter modules for PCR-targeting in *Saccharomyces cerevisiae*. Yeast 13, 1065–1075.

Wesp A, Hicke L, Palecek J, Lombardi R, Aust T, Munn AL, Riezman H (1997). End4p/Sla2p interacts with actin-associated proteins for endocytosis in *Saccharomyces cerevisiae*. Mol Biol Cell 8, 2291–2306.

Wilbur JD, Chen CY, Manalo V, Hwang PK, Fletterick RJ, Brodsky FM (2008). Actin binding by Hip1 (huntingtin-interacting protein 1) and Hip1R (Hip1-related protein) is regulated by clathrin light chain. J Biol Chem 283, 32870–32879.

Wilbur JD, Hwang PK, Ybe JA, Lane M, Sellers BD, Jacobson MP, Fletterick RJ, Brodsky FM (2010). Conformation switching of clathrin light chain regulates clathrin lattice assembly. Dev Cell 18, 841–848.

Winter D, Lechler T, Li R (1999). Activation of the yeast Arp2/3 complex by Bee1p, a WASP-family protein. Curr Biol 9, 501–504.

Wong MH, Meng L, Rajmohan R, Yu S, Thanabalu T (2010). Vrp1p-Las17p interaction is critical for actin patch polarization but is not essential for growth or fluid phase endocytosis in *S. cerevisiae*. Biochim Biophys Acta 1803, 1332–1346.

Wu M, Huang B, Graham M, Raimondi A, Heuser JE, Zhuang X, De Camilli P (2010). Coupling between clathrin-dependent endocytic budding and F-BAR-dependent tubulation in a cell-free system. Nat Cell Biol 12, 902–908.

Yang S, Cope MJ, Drubin DG (1999). Sla2p is associated with the yeast cortical actin cytoskeleton via redundant localization signals. Mol Biol Cell 10, 2265–2283.

Ybe JA, Greene B, Liu SH, Pley U, Parham P, Brodsky FM (1998). Clathrin self-assembly is regulated by three light-chain residues controlling the formation of critical salt bridges. EMBO J 17, 1297–1303.

Ybe JA, Perez-Miller S, Niu Q, Coates DA, Drazer MW, Clegg ME (2007). Light chain C-terminal region reinforces the stability of clathrin heavy chain trimers. Traffic 8, 1101–1110.

Ybe JA, Ruppel N, Mishra S, VanHaaften E (2003). Contribution of cysteines to clathrin trimerization domain stability and mapping of light chain binding. Traffic 4, 850–856.

Yeung BG, Phan HL, Payne GS (1999). Adaptor complex-independent clathrin function in yeast. Mol Biol Cell 10, 3643–3659.

Youn JY *et al*. (2010). Dissecting BAR domain function in the yeast amphiphysins Rvs161 and Rvs167 during endocytosis. Mol Biol Cell 21, 3054–3069.